DOI: 10.1002/((please add manuscript number))
Article type: Communication

Mechanically Robust and UV Curable Shape Memory Polymers for Digital Light Processing based 4D Printing

*Biao Zhang, Honggeng Li, Jianxiang Cheng, Haitao Ye, Amir Hosein Sakhaei, Chao Yuan, Ping Rao, Yuan-Fang Zhang, Zhe Chen, Rong Wang, Xiangnan He, Ji Liu, Rui Xiao, Shaoxing Qu, Qi Ge**

Prof. B. Zhang
Frontiers Science Center for Flexible Electronics (FSCFE), Xi'an Institute of Flexible Electronics (IFE) and Xi'an Institute of Biomedical Materials & Engineering (IBME), Northwestern Polytechnical University, 127 West Youyi Road, Xi'an 710072, China

Prof. B. Zhang, Dr. H. Li, J. Cheng, H. Ye., Prof. R. Wang, X. He, Prof. Ji Liu, Prof. Q. Ge
Shenzhen Key Laboratory of Biomimetic Robotics and Intelligent Systems, Department of Mechanical and Energy Engineering, Southern University of Science and Technology, Shenzhen, 518055, China
Guangdong Provincial Key Laboratory of Human-Augmentation and Rehabilitation Robotics in Universities, Southern University of Science and Technology, Shenzhen, 518055, China
E-mail: geq@sustech.edu.cn

Dr. A. H. Sakhaei
School of Engineering and Digital Arts,
University of Kent, Canterbury, Kent, CT2 7NT, United Kingdom

Prof. C. Yuan
State Key Laboratory for Strength and Vibration of Mechanical Structures, Department of Engineering Mechanics, Xi'an Jiaotong University, Xi'an 710049, China

Dr. P. Rao
Department of Mechanics and Aerospace Engineering,
Southern University of Science and Technology, Shenzhen, 518055, China

Dr. Y.-F. Zhang
Digital Manufacturing and Design Centre
Singapore University of Technology and Design, Singapore 487372, Singapore

Z. Chen, Prof. R. Xiao, Prof. S. Qu
State Key Laboratory of Fluid Power & Mechatronic System, Key Laboratory of Soft Machines and Smart Devices of Zhejiang Province, Department of Engineering Mechanics, Zhejiang University, Hangzhou 310027, China

B. Z., H. L., and J. C. contributed equally to this work.

Keywords: 4D printing, digital light processing, shape memory polymer, high stretchability

Abstract

Four-dimensional (4D) printing is an emerging fabrication technology that enables three-dimensionally (3D) printed structures to change configurations over "time" in response to the environmental stimulus. Compared with other soft active materials used for 4D printing, shape memory polymers (SMPs) have higher stiffness, and are compatible with various 3D printing technologies. Among them, ultraviolet (UV) curable SMPs are compatible with digital light processing (DLP)-based 3D printing to fabricate SMP-based structures with complex geometry and high-resolution. However, the UV curable SMPs have limitations in terms of mechanical performance, which significantly constraints their application ranges. Here, we report a mechanically robust and UV curable SMP system that is highly deformable, fatigue resistant, and compatible with DLP-based 3D printing to fabricate high-resolution (up to 2 μm), highly complex 3D structures that exhibit large shape change (up to 1240%) upon heating. More importantly, the developed SMP system exhibits excellent fatigue resistance and can be repeatedly loaded by more than 10,000 times. Substantial experimental investigations attribute the high stretchability to the combined effects of the high molecular weight of AUD crosslinker and the presence of hydrogen bonds. The development of the mechanically robust and UV curable SMPs significantly improves the mechanical performance of the SMP-based 4D printing structures which allows them to be applied to engineering applications such as aerospace, smart furniture, and soft robots.

Introduction

4D printing [1] is an emerging fabrication technology that enables 3D printed structures to change configurations over the fourth dimension "time" in response to the environmental stimulus including heat [2], moisture [3], magnetic field [4], electricity [5]. Due to its capability of seamlessly and rapidly fabricating actuator-mechanism integrated system, 4D printing is showing remarkable potential in aerospace [6], smart furniture [1a], minimal invasive devices [7], soft robots [8], and others [9]. 4D printing is realized by 3D printing structures with environmental responsive soft active materials (SAMs) which mainly include hydrogels [3, 10], liquid crystal elastomers (LCEs) [2b, 11], and shape memory polymers (SMPs) [2a, 7a, 9c, 12]. Different from the other two extremely soft SAMs (modulus of hydrogels ~1 to 100 kPa [3b, 13]; modulus of LCEs: ~100 kPa to ~MPa [2b, 11]), SMPs are capable of switching material modulus from a few MPa to a few GPa within one minute [14], and compatible with various 3D printing technologies. To date, SMP-based 4D printing has been widely applied to various areas including smart device [9c], origami [2a, 15], tissue engineering [16], metamaterial [17], biomedicine [7], and others [9a].

The current 3D printing technologies that are available for printing SMPs include Polyjet [2a], Fused Deposition Modeling (FDM) [12], Direct Ink Writing (DIW) [7b], Digital Light Processing (DLP)-based 3D printing [7a, 7d], Stereolithography (SLA) [12] and Two Photon Polymerization (TPP)[18]. However, most of the SMPs used for these 3D printing technologies are brittle at programming temperature (the temperature higher than SMP's phase transition temperature), which significantly constrains SMP-based 4D printing from engineering applications [9a]. For example, the commercial photopolymer Vero which has been widely used as SMP in Polyjet and DLP-based 3D printed could only be deformed by less than 30% at rubbery state [2a, 19]; the thermoplastic Polylactic Acid (PLA) which has been used as SMP in FDM and DIW-based 3D printed could only be stretched by less than 70% [7c, 20].

Compared with other printing technologies, DLP-based 3D printing enables the fabrication of SMP structures with high-resolution [17b] by employing digital mask projection that triggers the localized photopolymerization. In order to be compatible with DLP-based 3D printing, the SMP needs to be UV curable. Based on previous reports [7a, 9b, 9c, 17b, 21], the UV curable SMPs that are used for DLP-based 3D printing have limitations in terms of mechanical performance and printability, which significantly constraints their application ranges of 4D printed structures. For example, Choong et al. developed a *tert*-Butyl Acrylate (*t*BA)/Diethylene Glycol Diacrylate (DEGDA) SMP system which could be deformed by 50% at rubbery state [22]. Zarek et al. developed a UV curable semi-crystalline SMP by methacrylation of Polycaprolactone (PCL) which was applied to print flexible electronics due to its high stretchability (about 160%) [9c]. However, the methacrylated PCL is a vicious melt which requires heating assistance during printing process. We recently developed a methacrylate-based SMP system that enables high-resolution (up to 30 μm) and highly stretchable 4D printing (up to 300%), but the less reactive methacrylate functional group requires higher energy per unit area (~10-20 J/cm^2) to cure a layer, which significantly slows the printing speed [7a]. Moreover, the mechanical fatigue resistance is another key feature for the SMP-based 4D printing in engineering applications. However, the previous works barely investigated the fatigue resistance of 4D printing SMPs. Therefore, it is desired to develop UV curable SMPs which are highly deformable, and fatigue-resistant to remove the obstacles of implementing SMP-based 4D printing to engineering application.

Here, we report a mechanically robust and UV curable SMP system that is highly deformable, fatigue-resistant, and compatible with DLP-based 3D printing to fabricate high-resolution, highly complex 3D structures that exhibit large shape change upon heating. The SMP system is mainly consisted of *tert*-Butyl Acrylate (*t*BA) and Aliphatic Urethane Diacrylate (AUD), and thus named as *t*BA-AUD SMP system. The *t*BA-AUD SMP developed in this work can be

stretched by up to 1240% at programming temperature (i.e. 80 °C) (Movie S1), and this extremely large deformation can be fixed with an excellent shape fixity (~100%) at room temperature and recovered with a good shape recovery ratio (~90%) after heating back to 80 °C (Figure 1a, Movie S2). The developed SMP are highly UV curable (only requires 46.8 – 251.8 mJ/cm^2 to cure a layer), thus compatible with DLP-based 3D printing technology (Figure 1b) which enables the fabrication of high-resolution (up to 2 μm in Figure 1c), and highly complex 3D structures (Figure 1d). The robust mechanical performance of the *t*BA-AUD SMP allows us to program the printed 3D structures with extremely large tension, compression, and complex deformation (Figure 1e, f and Movie S3-S6) which can be repeatedly loaded by more than 10,000 times (Movie S7). More importantly, we conducted substantial experiments to investigate the large deformation mechanism of the *t*BA-AUD SMP system, and attribute its high stretchability to the combined effect of the high molecular weight of AUD crosslinker and the presence of hydrogen bonds. The development of *t*BA-AUD SMPs significantly improves the mechanical performance of the SMP-based 4D printing structures which allows them to be implemented to engineering applications.

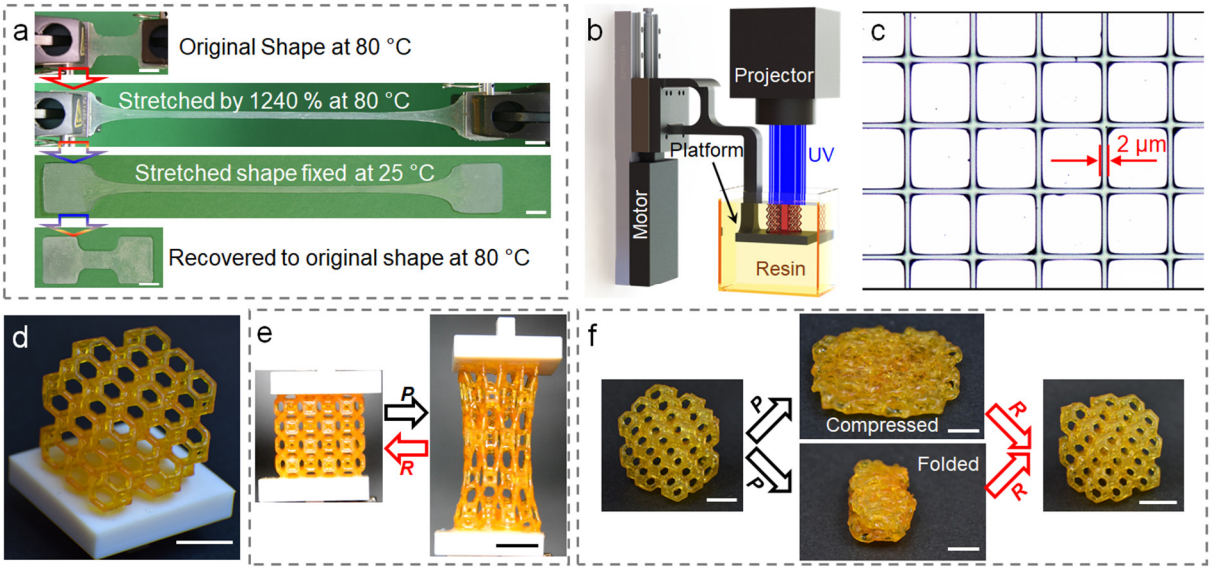

Figure 1. Mechanically robust *t*BA-AUD SMP for DLP-based 4D printing. (a) Snapshots of the shape memory cycle of a highly stretchable *t*BA-AUD SMP dog-bone sample. (b)

Schematic of DLP-based 3D printing apparatus. (c) Microscopic image of the grid pattern with 2 μm width printed with the *t*BA-AUD SMP. (d) A Kelvin foam printed with *t*BA-AUD SMP. (e) Demonstration of shape memory effect by stretching a Kelvin form. (f) Demonstration of shape memory effect by compressing and folding a Kelvin form. P: Programming; R: Recovery. Scale bar: 5 mm.

Figure 2a presents the chemicals that are used to prepare the *t*BA-AUD SMP precursor solution which consists of *tert*-Butyl Acrylate (*t*BA) as linear chain builder, Aliphatic Urethane Diacrylate (AUD) as crosslinker which is diluted by 33 wt% of Isobornyl Acrylate (IBOA), and Diphenyl(2,4,6-trimethylbenzoly) Phosphine Oxide (TPO) as photo initiator. DLP-based 3D printing fabricates 3D structure in a layer-by-layer manner, and each layer is formed by projecting digitalized UV patterns on the surface of polymer precursor solution to trigger the localized photopolymerization which transfers liquid solution into solid patterns. Figures 2b-d depict the DLP-based 3D printing associated photopolymerization of the *t*BA-AUD SMP system. The irradiation of UV lights activates photo initiator to generate free radicals that propagate through *t*BA, AUD and IBOA molecules (Figure 2b) which are chemically crosslinked to form covalent networks (Figure 2c) where the detailed chemical structure is presented in Figure 2d.

Due to the high molecular weight of the AUD crosslinker, its content highly affects the rheological behavior of *t*BA-AUD SMP precursor solution (Figure S1) which is critical to the DLP-based 3D printing process.[7d] The rheological characterization in Figure S2 indicates that all solutions with different AUD contents are Newtonian fluids at room temperature, and not dependent on testing frequency. As presented in Figure 2e, the increase in AUD content from 0 wt% to 100 wt% leads to the raise in viscosity from 0.01 Pa·s (10 cP) to 200 Pa·s (200,000 cP). Based on previous reports, the polymer solution with the viscosity higher than 3 Pa·s is not suitable for DLP-based 3D printing.[23] Therefore, we could only use the solution with AUD content that is not higher than 50 wt% to print SMP structures.

The AUD content does not only affect the viscosity of *t*BA-AUD SMP precursor solution, but also the kinetics and conversion of photopolymerization of the *t*BA-AUD SMP system which can be measured by the gel fraction characterizations.[24] Figure S3 presents a representative relation between gel fraction and irradiation energy (or curing time) (AUD content: 50 wt%). The gel fraction rapidly escalates to 92% with 0.35 J/cm^2 of UV irradiation energy (or 30 seconds), and equilibrates at this value even under longer curing time indicating that the *t*BA-AUD SMP system is well compatible with DLP-based 3D printing which requires fast kinetics of photopolymerization. We further investigate the effect of AUD concentration on the equilibrated gel fraction of the *t*BA-AUD SMP system with different AUD contents from 0 wt% to 50 wt%. As shown in Figure 2f, the equilibrated gel fraction gradually ramps from 0 % to ~90 % by increasing the AUD content from 0 wt% to 50 wt%. These gel fraction data could provide guidelines for estimating dynamic mechanical responses and predicting the stretchability at rubbery state of *t*BA-AUD SMP systems with different compositions.[24]

The UV light intensity is another key parameter that affects the kinetics of photopolymerization which can be reflected by the curing time during DLP-based 3D printing. As shown in Figure 2g, the ten times increase in UV light intensity from 2.46 mW/cm^2 to 25.18 mW/cm^2 results in about four times reduction in curing time; the *t*BA-AUD SMP system with higher content of AUD requires less UV curing time. More importantly, all the *t*BA-AUD SMP precursor solutions need less than 40 s to cure a 140 μm thick layer even under a weak UV light intensity (2.46 mW/cm^2). When the light intensity increases to 25.18 mW/cm^2, the curing times is reduced to shorter than 10 s even for the precursor solution with only 5 wt% of the AUD crosslinker. The short curing time to print a 140 μm thick layer further confirms that the *t*BA-AUD SMP system is suitable for DLP-based 3D printing. We note here that the energy per unit area that requires to cure a 140 μm thick layer of *t*BA-AUD SMP varies from 46.8 mJ/cm^2 to 251.8 mJ/cm^2 which is much lower that the energy per unit area (~10-20 J/cm^2) that is needed

to cure the previously reported methacrylate-based SMP which can be stretched by up to 300% [7a].

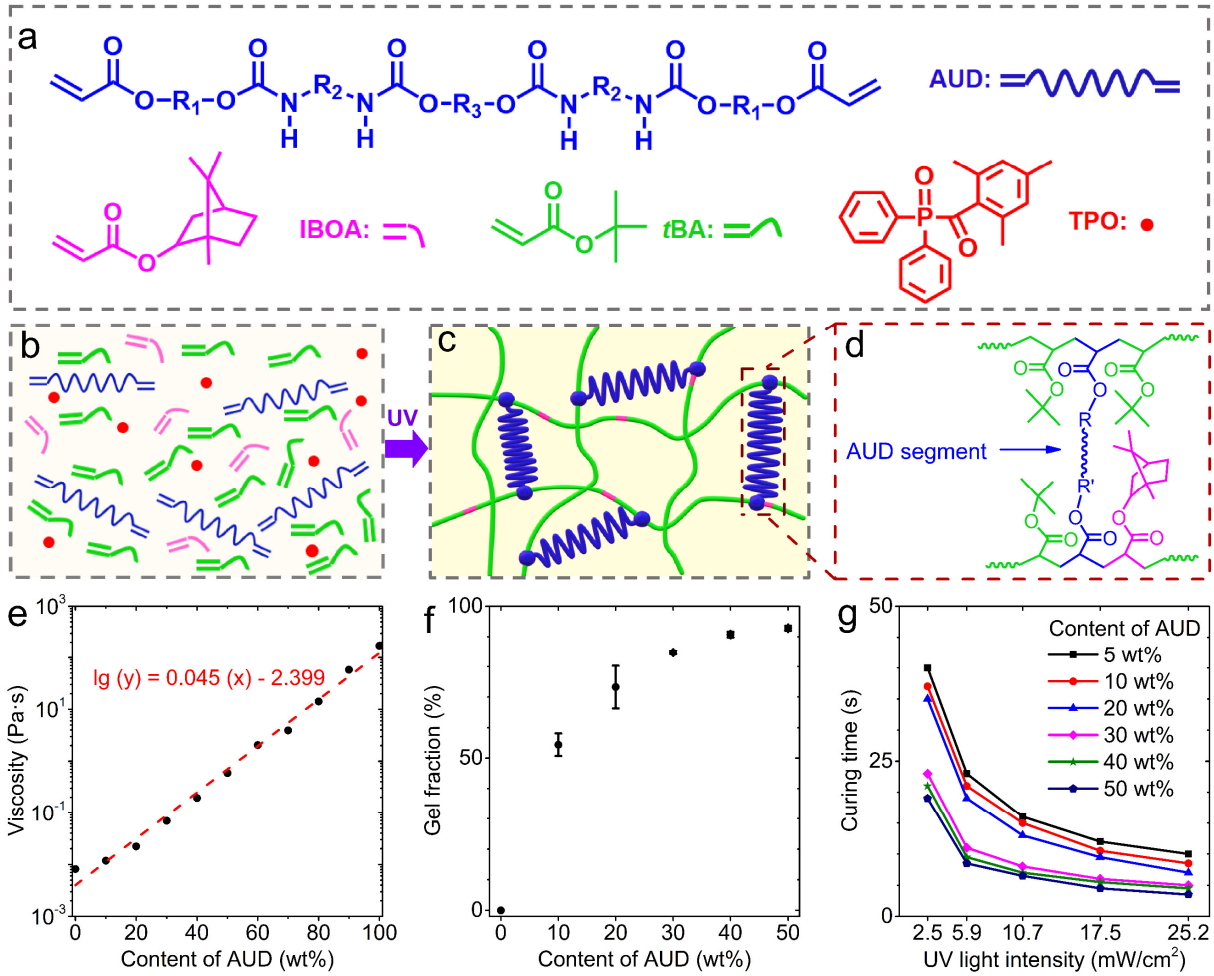

Figure 2. Details and characterizations of *t*BA-AUD SMP precursor solution. (a) Detailed chemical structures of AUD, *t*BA, IBOA and TPO that are used to prepare *t*BA-AUD SMP precursor solution. (b)-(d) Illustrations of the photopolymerization process during DLP-based 3D printing. (b) *t*BA-AUD SMP precursor solution before 3D printing. (c) *t*BA-AUD SMP network structure after 3D printing. (d) Detailed chemical structure of crosslinked *t*BA-AUD SMP. (e) Viscosity of *t*BA-AUD SMP precursor solution versus content of AUD. (f) Equilibrated gel fraction of *t*BA-AUD SMP changes versus content of AUD. (g) Curing times of *t*BA-AUD SMP with different contents of AUD versus UV light intensity.

To study the thermomechanical properties of *t*BA-AUD SMP system, we carried out dynamic mechanical analyses (DMA) on *t*BA-AUD SMP samples with different AUD contents. Figure S4 presents the temperature dependent storage modulus and tanδ of *t*BA-AUD SMP samples respectively. We identify glass transition temperature (T_g) at the peak of the corresponding tanδ

curve, and rubbery modulus from storage modulus curve at the temperature which is 30 °C higher than T_g. As summarized in Figure 3a, the increase in AUD content from 0 wt% to 50 wt% leads to: (i) the raise in rubbery modulus from 0.07 MPa to 1 MPa due to the increase in crosslinking density of the SMP system; (ii) the slight increases in T_g from 46.8 °C to 53.5 °C since higher crosslinking density results in lower polymer chain mobility, thus higher T_g. [25]

As the stretchability of *t*BA-AUD SMPs at rubbery state determines the deformation capability of 4D printed objects, we conducted the uniaxial tests for the *t*BA-AUD SMP system at high temperatures (T_g + 30 °C) to investigate the effect of AUD content on the stress-strain behavior at SMP's rubbery state. As presented in Figure 3b and summarized in Figure 3c, the reduction in AUD content from 50 wt% to 5 wt% results in a significant increase in the elongation-at-break from 272% to 1240%, but also a gradual decrease in Young's modulus from 1 MPa to 0.06 MPa. Moreover, we observe the hysteresis behavior on the stress-strain curve of the *t*BA-AUD SMP system (Figure S5a) as well as the residual strain after unloading which increases with the raise in AUD content (Figure S5b).

We further performed shape memory cyclic tests to examine the effect of AUD content on shape memory behavior of the *t*BA-AUD SMP system (Figure S6-S8). Figure 3d shows a representative shape memory cycle for the *t*BA-AUD SMP sample with 30 wt% AUD content. The SMP sample was first stretched by ε_p (ε_p = 100%) at the programming temperature (i.e. T_g+30 °C, and it is 80 °C in this case). Then, the temperature was gradually decreased to 25 °C while keeping the sample stretched by 100%; after reaching 25 °C, the sample was held isothermally for 2 min. The temporary fixed strain ε_u was achieved by suddenly removing the external load. The free recovery was activated by gradually increasing the temperature to the recovery temperature (80 °C), and the recovery strain ε_r was measured. We calculate the shape fixing ratio R_f ($R_f = \varepsilon_u / \varepsilon_p$) and shape recovery ratio R_r ($R_r = (\varepsilon_u - \varepsilon_r) / \varepsilon_u$) to quantify the

shape fixing and recovery capabilities. Figure 3e summaries the effect of AUD content on R_f and R_r extracted from Figure 3d and Figure S6: R_f is above 99% with different AUD contents; R_r is about 95.5% when the AUD content is 0 wt%– 30 wt%, and declines to 86% after increasing the AUD content to 50 wt% which is consistent with the tendency in residual strain with the increase in AUD content (Figure S5). We also examined the shape memory behaviors of the *t*BA-AUD SMPs when they were stretched by large deformations (90% of Elongation-at-break). As shown in Figure S7, all the SMP samples exhibit excellent shape fixities (~100%) and good shape recovery ratios (>80%) even under extremely large deformations.

Beside the high stretchability at rubbery state, the *t*BA-AUD SMP system also exhibits excellent mechanical repeatability and fatigue resistance. To demonstrate this, we conducted the fatigue test on a *t*BA-AUD SMP sample with 10 wt% AUD content at 80 °C with a cyclic strain from 150% to 250% at a frequency of 0.25 Hz. As presented in Figure 3f, the *t*BA-AUD SMP sample can sustain more than 10,000 loading cycles without fracture (Movie S7). In contrast, the previous reported UV curable SMPs such as *Vero* (Figure S9), *t*BA-PEGDA (PEGDA: Poly(ethylene glycol) Diacrylate; Figure S10), and BMA-PEGDMA (BMA: Benzyl Methacrylate; PEGDMA: Poly(ethylene glycol) Dimethacrylate; Figure S11), could only bear less than 100 loading cycles with much lower strain amplitude (for Vero and *t*BA-PEGDA, the strain range is 10% to 20%; for BMA-PEGDMA, the strain range is 20% to 40%).

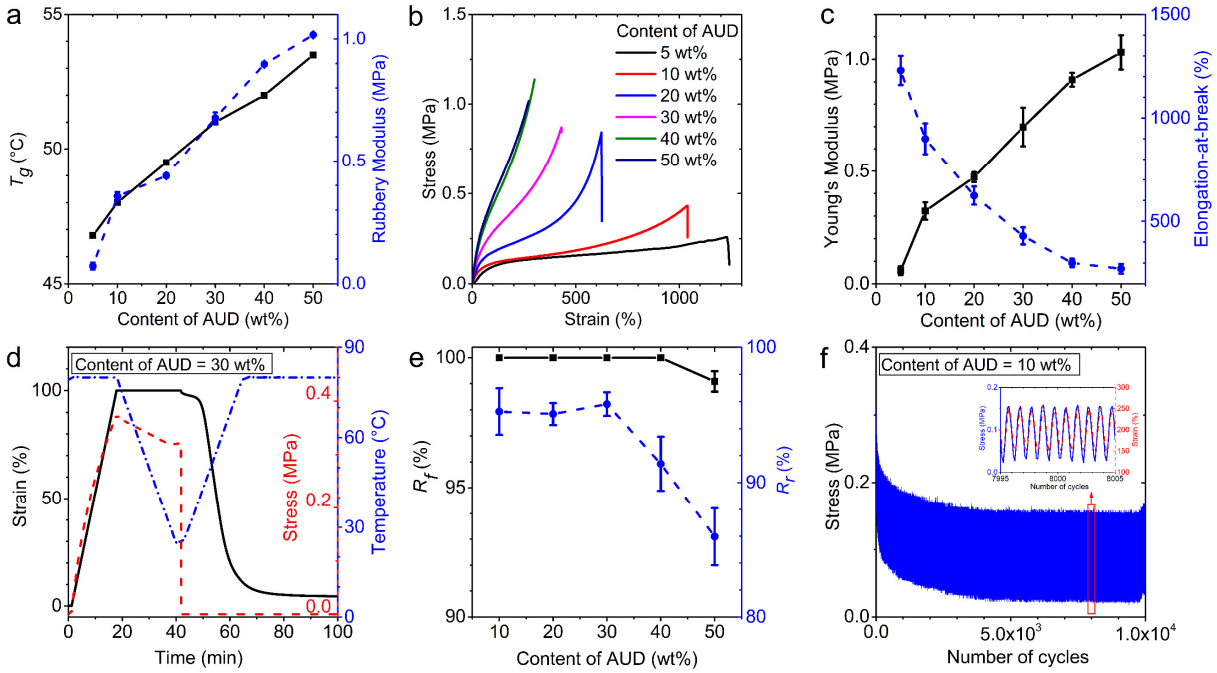

Figure 3. Thermomechanical property of the *t*BA-AUD SMP system. (a) Glass transition temperature (T_g) and rubbery modulus versus content of AUD extracted from DMA tests. (b) Stress-strain behavior of the *t*BA-AUD SMP with different AUD content. (c) Young's modulus and elongation-at-break versus content of AUD; (d) Representative shape memory behavior of a *t*BA-AUD SMP sample with 30 wt% AUD content. (e) Shape fixing ratio R_f and shape recovery ratio R_r versus content of AUD. (f) Fatigue test of a *t*BA-AUD SMP sample with 10 wt% AUD content.

Different from the previously reported UV curable SMP systems, the AUD crosslinker plays a key role to impart the high deformability and fatigue resistance to the *t*BA-AUD SMP system. As illustrated in Figure 4a, we attribute the high stretchability to the combined effects of the high molecular weight of AUD crosslinker and the presence of hydrogen bonds: (i) high molecular weight of AUD crosslinker greatly increases the average distance between crosslinking points, which significantly raises the stretchability of the system; (ii) some of the long linear chains formed by *t*BA are coiled and trapped between the AUD crosslinkers which are attracted by the hydrogen bonds; (iii) large deformation breaks the hydrogen bonds, which releases the coiled long linear chains so that the material can be stretched further by larger deformation; (iv) after unloading, some of the large deformation can be recovered due to entropic elasticity, while the recovery of broken hydrogen bonds takes longer time so that the residual strain can be observed as some of the long linear chains cannot return to their original

coiled shape; (v) residual strain can be eliminated by thermal treatment which accelerates the recovery of hydrogen bonds and increases the mobility of the long linear chains. We further validate the proposed deformation mechanism by conducting substantial experiments.

Figure 4b presents the results from gel permeation chromatography (GPC) test confirming that AUD is a high molecular weight crosslinker (M_n = 31148) with decent polydispersity (PDI = 1.39). Details on the GPC test can be found in Experiment Section. The high molecular weight of AUD crosslinker increases the average distance between crosslinking points, thus the stretchability of the system. To validate this point, we performed uniaxial tensile tests (Figure S12a) on the *t*BA-PEGDA SMP system whose crosslinker has much lower molecular weight (PEGDA's M_n is 700), and compared the relation of elongation-at-break and Young's modulus between *t*BA-AUD system and *t*BA-PEGDA system. As shown in Figure S12b, at the same Young's modulus (i.e., the same crosslinking density), the stretchability of the *t*BA-AUD SMP system is three to seven times higher than that of the *t*BA-PEGDA SMP system.

To validate the presence of hydrogen bonds, we performed Fourier Transformation Infrared Spectroscopy (FTIR) tests (Figure S13, Figures 4c and d). As shown in Figure 4c, the C=O group stretching of the pure *t*BA sample (AUD content: 0 wt%) is at 1724 cm^{-1}, and the increase in the AUD content shifts the C=O group stretching to lower wavenumber due to the presence of hydrogen bonds between the C=O and N-H groups (Figure S14).[8b, 26] More importantly, the 10,000-cycle fatigue loading makes the C=O peak shape become narrow and slightly shift to the left. Moreover, from the wavenumber range from 3200 - 3400 cm^{-1} in Figure 4d, we could only observe the overtone stretching of the C=O group at 3430 cm^{-1} from the pure *t*BA sample,[27] and the stretching of the N-H group at 3384 cm^{-1} from the pure AUD sample; from the *t*BA-AUD SMP samples, we can observe both the stretching bands from the C=O group and the N-H group, but the stretching of the C=O group becomes broader, and the stretching of the N-H group shifts to lower wavenumber due to the presence of hydrogen bonds.[8b, 26] Again,

the fatigue cyclic loading weakens vibration peaks located at 3384 cm^{-1} and 3430 cm^{-1}. In addition, the presence of hydrogen bonds can also be validated by comparing the Amide III (C-N) bands between *t*BA-AUD SMPs with different AUD contents (Figure S15).

The presence of hydrogen bonds can be further validated by conducting stress relaxation test on a fresh *t*BA-AUD sample with 10 wt% of AUD crosslinker. As shown in Figure 4e, by stretching the sample by 100%, we can observe apparent stress relaxation which is attributed to the breakage of hydrogen bonds. The stress relaxation can be also observed in the fatigue test shown in Figure 3f where the stress levels out after 4,000 cycles indicating all the hydrogen bonds are broken. To validate this point, we also conducted the stress relaxation test on the sample after the 10,000-cycle fatigue test, and find the stress relaxation behavior disappears (Figure 4e). Moreover, the breakage of hydrogen bonds leads to significant residual strain. As shown in Figure 4f, the gauge length of the sample increases from 20 mm to 39.8 mm resulting in a 99% of residual strain after the 10,000 cyclically loading between 150% and 250%. This is because the breakage of hydrogen bonds makes some of the long linear chains unable to return to the original coiled shape. The breakage of the hydrogen bonds can be recovered by heating the SMP with 99% of residual strain at 120 °C for 12 hours. Figure 4e shows that the recovered sample exhibits nearly identical stress relaxation behavior as the fresh SMP shape. Figure 4f presents that the heating treatment makes the sample eliminate the residual strain.

To validate the contribution of hydrogen bonds to the stretchability of the *t*BA-AUD SMP system, we performed uniaxial tensile tests on the fresh sample as well as the sample after 10,000-cycle fatigue test where all the hydrogen bonds are broken. As presented in Figure 4g, the fresh sample breaks at 1040% while the sample after 10,000-cycle fatigue test ruptures at 470%, which is because the original length of the 10,000-cycle loaded sample is two times of the fresh sample. We also observe that stiffness of the sample after the fatigue test is lower at low strain range (less than 200%) due to the breakage of hydrogen bonds, but both samples

break at similar stress (~0.4 MPa) and length (~227 mm) indicating the factures of both samples are eventually resulted from the ruptures of the same macromolecular structure. Moreover, we compare the shape memory behaviors between the fresh and cyclically loaded SMP samples. As shown in Figure S8a, even after heating at 80 °C for 1 hour, we could still observe ~40% residual strain on the fresh SMP sample due to the existence of the hydrogen bonds in the fresh SMP sample. In contrast, as shown in Figure S8b, the cyclically loaded SMP sample is able to recover all the strain as the cyclic loads have broken all the hydrogen bonds, and eliminated the residual strain caused by the breakage of hydrogen bonds.

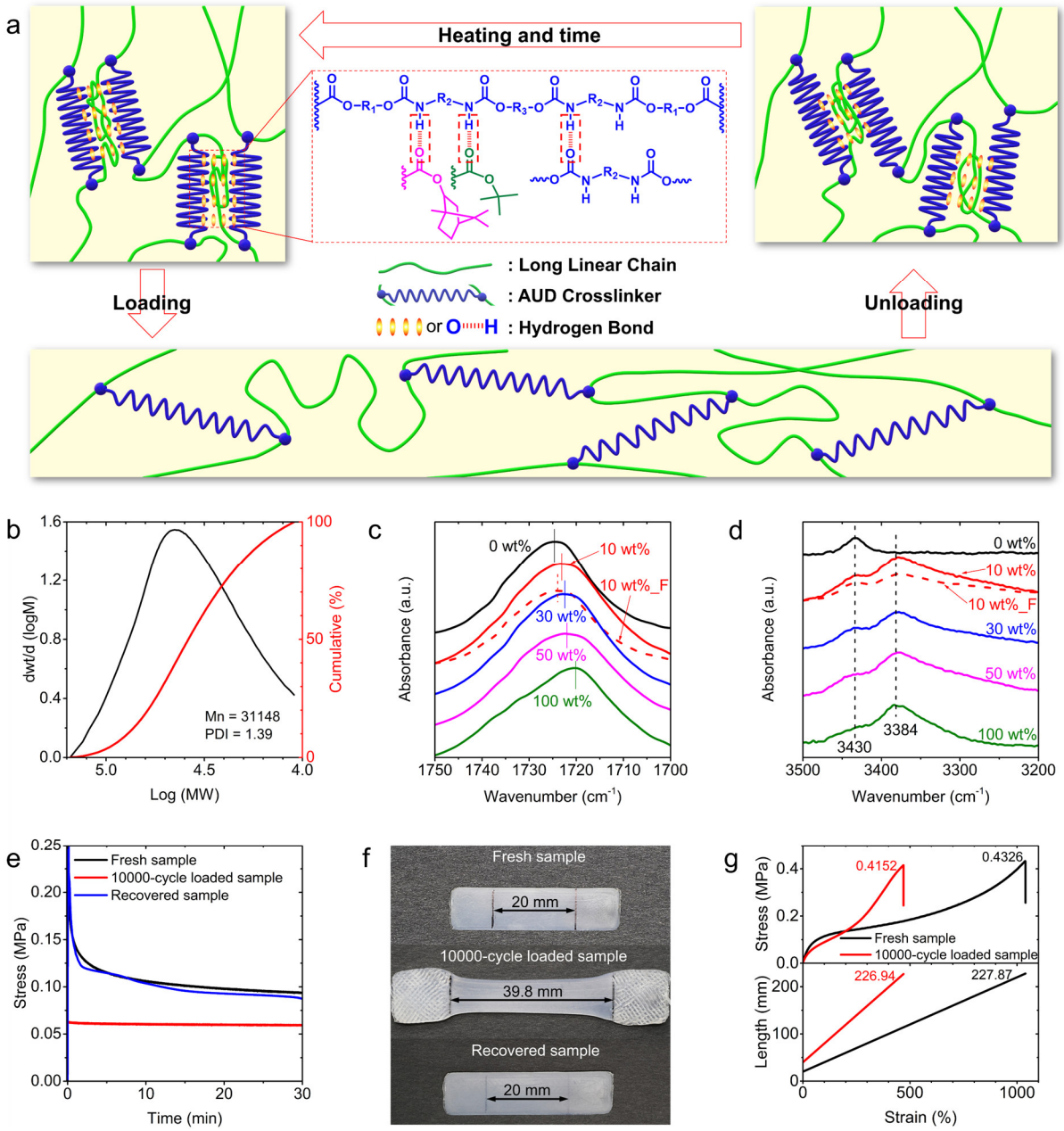

Figure 4. Deformation mechanism for the stretchability of the *t*BA-AUD SMP system. (a) Illustration on the deformation mechanism. (b) GPC testing result. (c) and (d) FTIR spectrum at the ranges of 1800-1650 cm^{-1} and 3500-3200 cm^{-1} respectively (10 wt%: 10 wt% of AUD; 10 wt%_F: the 10 wt% SMP with the 10,000-cycle fatigue test). (e) Stress relaxation testing results. (f) Comparison on the gauge length of one sample after different treatments. (g) Comparison on uniaxial tensile tests between the fresh *t*BA-AUD SMP sample and the one after 10,000-cycle fatigue test.

The chart presented in Figure 5a summaries the Elongation-at-break of the SMPs suitable with different 3D printing technologies. Details can be found in Supplementary Materials Table S1 and Figure S16-S20. Thanks to the compatibility with DLP-based 3D printing, the *t*BA-AUD

SMPs can be used to fabricate high-resolution SMP structures (up to 2 μm). More importantly, compared with other SMPs, the *t*BA-AUD SMPs exhibit the extremely high deformability (up to 1240%) at rubbery state, which allows us to print thick beams with large bendability. To demonstrate this, we first print a "L" shape beam with 10 mm thickness (picture (ii) in Figure 5b) of which we fix the blue end and bend the red end in counterclockwise direction to form a "U" shape beam (picture (i) in Figure 5b); we achieve the "I" shape beam by bending the red end in clockwise direction (picture (iii) in Figure 5b), and another "U" shape beam by further bending the red end in clockwise direction (picture (iv) in Figure 5b). Figure 5c presents the corresponding Finite Element (FE) simulations that predict strain contour maps for each bending case. FE simulations reveal that the large deformations occur during bending the "L" shape thick beam. Especially, to achieve the "U" shape in the picture (iv) of Figure 5b, the maximum principal strain on the beam is ~280% which is higher than the elongation-at-break of most previously reported 3D printable SMPs (Figure 5a).

The high deformability makes the *t*BA-AUD SMP an idea material to fabricate smart furniture with SMP hinges. Figure 5d presents a 3D printed SMP hinge with lattice microstructure. As shown in Figure 5e, we can program the SMP lattice hinge into a folded shape due to its high deformability and shape memory effect. In Figure 5f, we further build a smart table where the eight SMP lattice hinges connect the table board and legs. The shape memory effect of the SMP lattice hinges enable the smart table to be programmed into a compact 2D board (Figure 5g), which significantly saves the space for storage and transportation. When in use, the SMP hinges open spontaneously upon heating (Figure 5g and Movie S8), and the smart table is able to support heavy load (Figure 5h) due to *t*BA-SMP's high stiffness at room temperature (Figure S21).

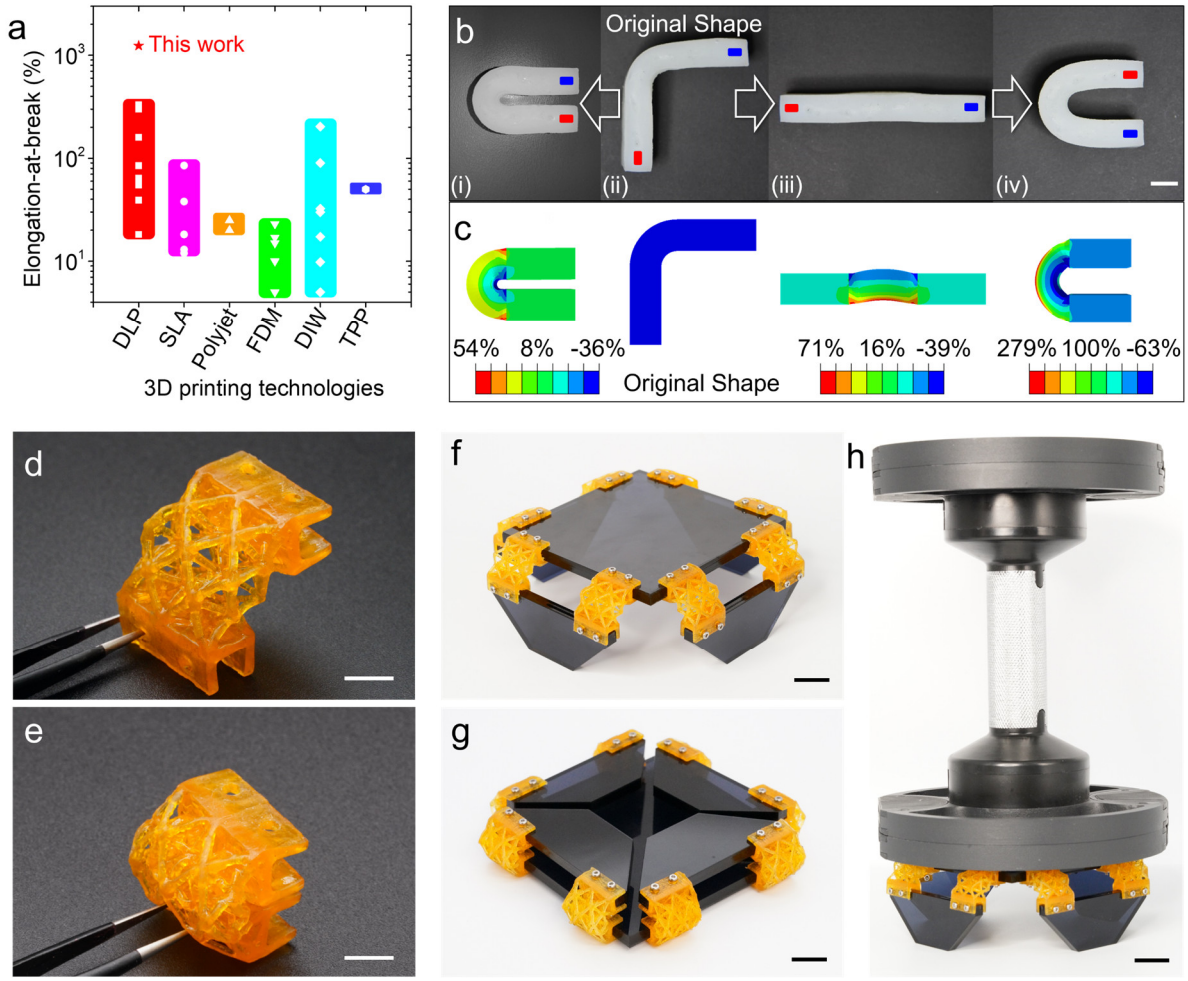

Figure 5. Highly deformable *t*BA-AUD SMP and its engineering application in smart furniture. (a) Chart summarizing the Elongation-at-break of the SMPs suitable with different 3D printing technologies to compare the mechanical performance of *t*BA-AUD SMPs with those of previously reported 3D printable SMPs. (b) Demonstrations that show large deformations of a thick "L" shape beam made of *t*BA-AUD SMP. (c) The corresponding FE simulations for the cases in (b). (d) Snapshot of a printed SMP lattice hinge at the as-printed shape. (e) Snapshot of a printed SMP lattice hinge at the temporary folded shape. (f) Snapshot of the smart table consisting of eight SMP lattice hinges connecting the table board and four legs. (g) The smart table programmed into a 2D compact shape. (h) Demonstration that shows the smart table is able to support heavy load. Scale bars in (b), (d), (e): 10 mm; scale bars in (f)-(h): 20 mm.

Moreover, the *t*BA-AUD SMP also shows great potentials in aerospace applications. Figure 6a demonstrates the design of a SMP smart hinge with micro channels where the resistance wire can pass through (Figure 6b). As illustrated in Figure 6c, the folded shape of the smart hinge can recover to its original straight shape through Joule heating. [19b] Figure 6d presents the printed smart hinge where its micro-channels are shown in Figure 6e. Figures 6f and g demonstrate the straight and folded shapes of the smart hinge with a resistance wire. Figures

6h-k present the Joule heating activated recovery process of the smart hinge. We applied a 3.7 A current to heat the hinge. The hinge was heated to 80°C and recovered to its original straight shape within 1 min (Movie S9). We further used the SMP smart hinge to make the deployable solar panels. As shown in Figure 6l, the SMP hinge connected solar panels can be folded in the storage mode. The Joule heating triggered the quick deployment of the solar panels (Figure 6m and Movie S10) which can generate electricity to power a motor and lighten a LED (Figure 6l and Movie S11).

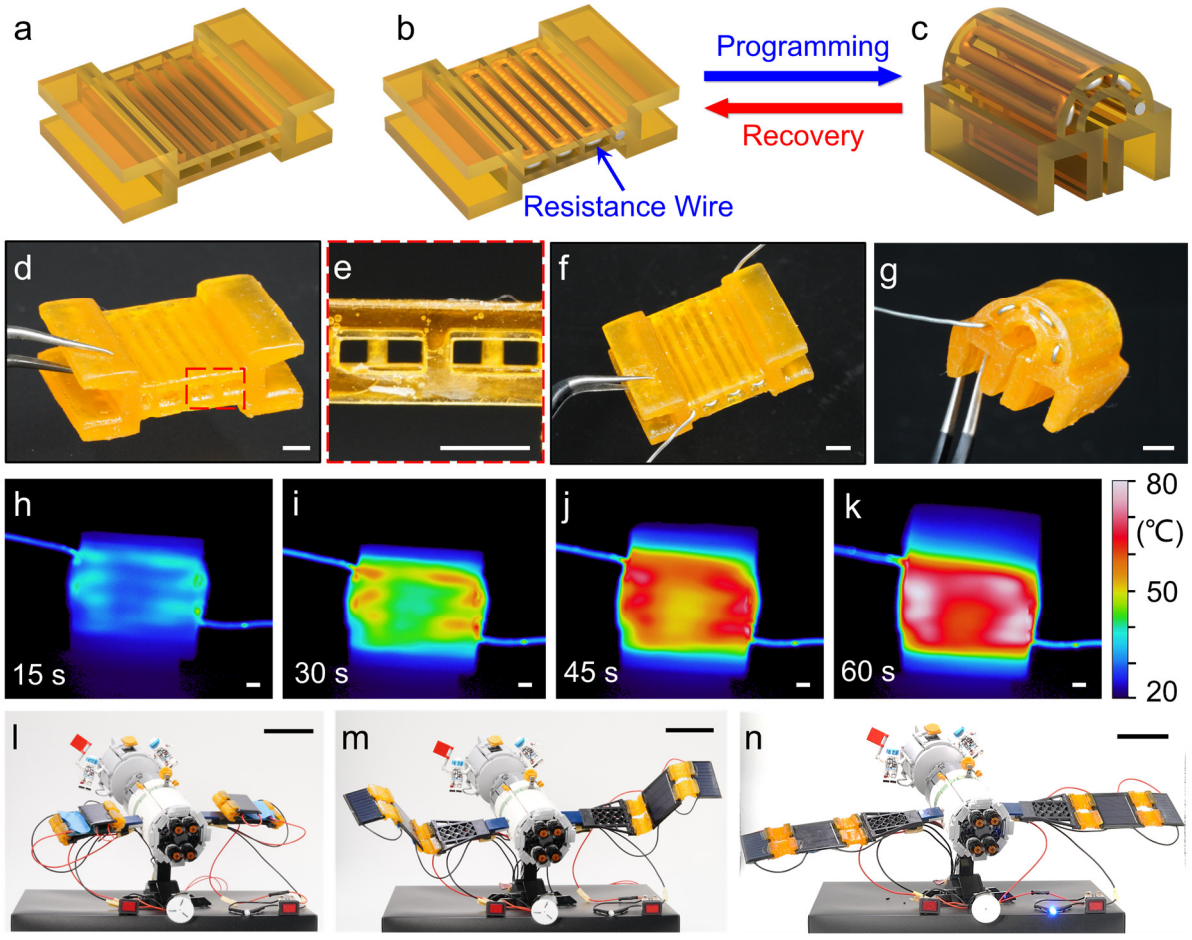

Figure 6. Demonstration of the application of *t*BA-AUD SMP to aerospace. (a)-(c) Illustrations on the design of the design of a SMP smart hinge with micro channels where the resistance wire can pass through for Joule heating. (d)-(g) Th corresponding snapshots of the printed SMP smart hinge. (h)-(k) Inferred images capturing the Joule heating activated recovery. (l)-(n) Demonstrations of the SMP smart hinge-based deployable solar panels. (l) A spacecraft with solar panels under compacted shape. (m) Deployment process of the solar panels (n) Fully

deployed the solar panels that generate electricity to power a motor and lighten a LED. Scale bars in (d)-(k) 2 mm; scale bars in (l)-(n): 5 cm.

In summary, we report a mechanically robust and UV curable shape memory polymer system which is compatible with DLP-based 3D printing system to fabricate 4D printed structures with high-resolution and highly complex geometry. The *t*BA-AUD SMP system mainly consists of *tert*-Butyl Acrylate (*t*BA) as linear chain builder and Aliphatic Urethane Diacrylate (AUD) as crosslinker. The AUD crosslinker endows high deformability and fatigue resistance to the *t*BA-AUD SMP system so that the printed samples can be stretched by up to 1240% and repeatedly loaded by more than 10,000 times. We conduct comprehensive experiments to investigate to the effects of AUD crosslinker on the thermomechanical properties such as dynamic mechanical performance, stress-strain relation, shape memory behavior and fatigue resistance of the *t*BA-AUD SMP system. We also propose deformation mechanism of the highly deformable *t*BA-AUD SMP system which is resulted from the combined effect of high molecular weight of AUD crosslinker and the presence of hydrogen bonds. We carry out experiments to successfully prove our hypothesis. Finally, we demonstration two applications to show the potentials of *t*BA-AUD SMPs in the areas of smart furniture and aerospace.

Experimental Section

Materials

Tert-butyl acrylate (*t*BA), Diphenyl(2,4,6-trimethylbenzoly) phosphine oxide (TPO) and Sudan I were purchased from Sigma-Aldrich (Singapore) and used without further purification. Aliphatic urethane di-acrylate (AUD, Ebecryl 8413) was kindly provided by Allnex (Germany).

Precursor solution preparation

The highly stretchable shape memory polymer resin was prepared by mixing *t*BA and AUD in different composition. 2 wt% TPO of total weight of monomer and crosslinker was added as the photoinitiator. In some cases, 0.02 wt% Sudan I of total weight of the polymer resin was added as photo absorber to improve the printing resolution.

3D printing

The UV curable solutions we prepared were printed by Digital Light Processing (DLP) method. A custom-built microlithography system, of which the light source is 405 nm, was used in this study.[7a] 3D structure images in STL version were firstly sliced into layers with the target thickness and the printing parameters were set by using the custom LabVIEW. The structure was printed layer by layer exposing under UV light. The grid structure in Figure 1c was printed using a commercial 3D printer (405 nm, nanoArch P130 3D printing system, BMF Material, China). The demonstrations in Figure 5 and Figure 6 were printed on a self-built 3D printer with printing resolution of 17.6 μm/pixel and printing area of 34 mm × 19 mm. After printing, the surface of the obtained 3D structures was cleaned by a rubber suction bulb. Finally, the structures were post-cured by putting into a UV oven (365 nm, UVP, Ultraviolet Crosslinkers, Upland, CA, USA).

Characterization

Rheological measurements

The viscosity (η) of all samples was measured by using a controlled-stress rheometer (DHR2, TA instruments Inc., UK) with an aluminum plate geometry (diameter 40 mm, gap 500 μm). All dynamic rheological data were checked as a function of strain amplitude to ensure that the measurements were performed in the linear domain. A particular care was taken in order to prevent the moisture uptake during measurements by using a homemade cover.

Gel fraction test

The prepared strip samples with the weight around 100 mg were put into the vials with approximately 20 mL of acetone separately. Acetone was chosen as the solvent as the tBA monomer, AUD crosslinker, and Poly(tBA) were all well soluble in acetone. The vials were allowed to soak for one week to allow all noncrosslinked materials to be removed from the network polymer. The residues of strips were then removed from the acetone and placed in the oven at 60 °C for 24 h to drive off the remaining solvent. Then the obtained samples were exposed under air for 24 h. The weight of the final left polymer was measured and the gel fraction was calculated by the following equation:

$$\text{Gel fraction (\%)} = W_{\text{left}}/W_{\text{total}} \times 100\%$$

Here, W_{total} represents the initial weight of the sample and W_{left} represents the weight of the final left polymer. Three samples of each polymer were measured to prove the repeatability.

Curing time

To evaluate the 3D printing ability, the curing time of *t*BA-AUD SMP system was studied. Firstly, the prepared *t*BA-AUD SMP pre-polymer solution was sandwiched between two glass slides with a gap of 140 μm, and then the patterned near UV light with 405 nm wavelength was irradiated. The curing time was recorded when a *t*BA-AUD SMP based pattern can be visually

observed. The effect of luminous intensity on curing time was also investigated by varying the light source intensity from 2.46 mW/cm^2 to 25.18 mW/cm^2.

Gel permeation chromatography tests

The molecular weight of AUD was measured by using ACQUIITY Advanced Polymer Chromatography (APC) system (Waters) and DMF/LiCl (10 mM) as the eluent. The temperature was set at 50 °C and the flow rate of eluent was 0.5 mL/min. The sample was prepared in DMF/LiCl and filtered through 0.20 μm pore size PTFE filter prior to the measurements. Molecular weight data was determined by using the response of differential refractive index detector and was calibrated with PMMA standard (3000 g/mol – 70000 g/mol).

Fourier Transformation Infrared Spectroscopy

The Fourier transform infrared (FTIR) spectra were recorded using a FTIR spectrophotometer (Nicolet iS50 FT-IR Spectrometer, Thermo Scientific) in conjunction with platinum ATR single-reflection diamond accessory collecting 32 scans (resolution, 4 cm^{-1}) from 400 to 4000 cm^{-1}.

Dynamic mechanical analysis experiments

Dynamic mechanical properties were studied by using a dynamic mechanical analysis (DMA) analyzer (Q800 DMA, TA Instruments) in the tension film mode. Samples for all the compositions were trimmed to a typical dimension of 15 mm × 5 mm × 1.0 mm and tested at a frequency of 1 Hz, a "force track" of 125% and an amplitude of 15 μm. The temperature was first increased to 100 °C, held isothermally at 100 °C for 10 min to eliminate the thermal history. Then the temperature was cooled down at a heating rate of 2 °C/min. The glass transition temperatures (T_g) were assigned as the temperature at which tanδ value is maximum. Each composition was tested at least two times to ensure the repeatability.

Uniaxial tensile experiments

Tension experiments on rectangular specimens with dimensions of 15 mm × 5 mm × 1.0 mm were conducted using MTS machine (100 N load cell, USA) with a thermal chamber at strain rate of 1%/s. The test temperature was set at T_g +30 °C of the corresponding specimen.

Shape memory behavior tests

The shape memory (SM) behavior of the materials was investigated by following a typical shape memory cycling method. The sample was first stretched to 100% with a constant loading rate (6.00 %/min) at a programming temperature (i.e. T_g+30 °C), and then the temperature was decreased to room temperature (25 °C) with a cooling rate at 2 °C/min. After reached the target temperature, the sample was held isothermally for 2 min. By following the tensile was removed. In the free recovery step, the temperature was gradually increased to the recovery temperature (i.e. T_g+30 °C) at the rate of 2 °C/min. the sample was held isothermally for another 60 min.

Fatigue tests

In order to evaluate the fatigue resistance of the material, tensile fatigue tests of *t*BA:AUD = 9:1, Vero, *t*BA:PEGDA = 9:1 and BMA:PEGDMA = 9:1 were carried out using an ElectroForce machine (ET1-2, TA Instruments) at T_g + 30 °C. All test samples are 20 mm × 5 mm × 2 mm (stretch section length is 10 mm) and at least three samples are to be tested for each sample. Firstly, the distance between the two clamps is set to 10 mm with the upper clamp holding the sample, and the lower clamp opens. The oven was then raised to 80 ° C and kept for 5 minutes. Next, the sample was loaded and the cyclic tensile test was started. Samples with 10 wt% of AUD are slowly stretched to 35 mm (250% strain) and then restored to 25 mm (150% strain). Then this cycle experiment was repeated for 10 000 times with the frequency of 0.25 Hz and the strain amplitude of 150% -250%. The fatigue test of Vero and *t*BA-PEGDA used

the same protocols with the frequency of 0.25 Hz and the strain amplitude of 10% - 20%. The fatigue test of BMA-PEGDMA used the same protocols with the frequency of 0.25 Hz and the strain amplitude of 20% - 40%.

Loading-unloading cyclic tests

According to the tensile test results, two materials with similar Young's modulus (*t*BA:AUD = 5:5 and *t*BA: PEGDA = 19:1) were selected for loading-unloading test to compare and analyze different cross-linking materials. Using Dynamic mechanical analysis (DMA, Q800 DMA, TA Instruments), 5%, 10%, 15% and 20% strains were stretched with four sets of samples at T_g + 30 °C at a strain rate of 10%/min. Then, the stress is unloaded at the same rate. For the material *t*BA: AUD = 5:5, a set of large strain loading-unloading tests was added, and 50%, 100%, 150%, 200%, 250% and 300% were completed at a strain rate of 100%/min. A cyclic experiment of variables. All samples were trimmed to a size of 15 mm × 5 mm × 0.5 mm.

Simulation

To investigate the local strains on the deformed printed structures, the finite element simulations were performed using a commercial FE software ABAQUS (Simulia, Providence, RI, USA). The geometries were meshed using 8-node linear brick, hybrid, constant pressure (C3D8H). The Mooney‐Rivlin model was used to capture the hyperelastic behavior of the *t*BA-AUD SMPs at rubbery state.

Supporting Information

Supporting Information is available from the Wiley Online Library or from the author.

Acknowledgements

B.Z., H.L., and J.C. contributed equally to this work. Q.G. acknowledges the National Natural Science Foundation of China (No. 12072142), and the supported by the Science, Technology and Innovation Commission of Shenzhen Municipality under grant no.

ZDSYS20200811143601004. B.Z. acknowledges the National Natural Science Foundation of China (No. 51903210) and Natural Science Basic Research Program of Shaanxi (Program No. 2020JQ-174).

Received: ((will be filled in by the editorial staff))
Revised: ((will be filled in by the editorial staff))
Published online: ((will be filled in by the editorial staff))

References

[1] a) S. Tibbits, presented at TED conference **2013**; b) Q. Ge, H. J. Qi, M. L. Dunn, *Applied Physics Letters* **2013**, 103, 131901.

[2] a) Z. Ding, C. Yuan, X. Peng, T. Wang, H. J. Qi, M. L. Dunn, *Sci Adv* **2017**, 3, e1602890; b) A. Kotikian, R. L. Truby, J. W. Boley, T. J. White, J. A. Lewis, *Adv Mater* **2018**, 30, 1706164.

[3] a) D. Raviv, W. Zhao, C. McKnelly, A. Papadopoulou, A. Kadambi, B. Shi, S. Hirsch, D. Dikovsky, M. Zyracki, C. Olguin, R. Raskar, S. Tibbits, *Sci Rep* **2014**, 4, 7422; b) A. S. Gladman, E. A. Matsumoto, R. G. Nuzzo, L. Mahadevan, J. A. Lewis, *Nat Mater* **2016**, 15, 413.

[4] Y. Kim, H. Yuk, R. Zhao, S. A. Chester, X. Zhao, *Nature* **2018**, 558, 274.

[5] J. N. Rodriguez, C. Zhu, E. B. Duoss, T. S. Wilson, C. M. Spadaccini, J. P. Lewicki, *Sci Rep* **2016**, 6, 27933.

[6] K. Liu, J. Wu, G. H. Paulino, H. J. Qi, *Sci Rep* **2017**, 7, 3511.

[7] a) Q. Ge, A. H. Sakhaei, H. Lee, C. K. Dunn, N. X. Fang, M. L. Dunn, *Sci Rep* **2016**, 6, 31110; b) H. Wei, Q. Zhang, Y. Yao, L. Liu, Y. Liu, J. Leng, *ACS Appl Mater Interfaces* **2017**, 9, 876; c) C. Lin, J. Lv, Y. Li, F. Zhang, J. Li, Y. Liu, L. Liu, J. Leng, *Advanced Functional Materials* **2019**, 29, 1906569; d) B. Zhang, W. Zhang, Z. Zhang, Y. F. Zhang, H. Hingorani, Z. Liu, J. Liu, Q. Ge, *ACS Appl Mater Interfaces* **2019**, 11, 10328.

[8] a) M. D. N. I. Shiblee, K. Ahmed, M. Kawakami, H. Furukawa, *Advanced Materials Technologies* **2019**, 4, 1900071; b) D. K. Patel, A. H. Sakhaei, M. Layani, B. Zhang, Q. Ge, S. Magdassi, *Adv Mater* **2017**, 29, 1606000.

[9] a) X. Kuang, D. J. Roach, J. Wu, C. M. Hamel, Z. Ding, T. Wang, M. L. Dunn, H. J. Qi, *Advanced Functional Materials* **2019**, 29, 1805290; b) M. Zarek, N. Mansour, S. Shapira, D. Cohn, *Macromol Rapid Commun* **2017**, 38, 1600628; c) M. Zarek, M. Layani, I. Cooperstein, E. Sachyani, D. Cohn, S. Magdassi, *Adv Mater* **2016**, 28, 4449; d) L. Huang, R. Jiang, J. Wu, J. Song, H. Bai, B. Li, Q. Zhao, T. Xie, *Adv Mater* **2017**, 29, 1605390.

[10] a) Y. Mao, Z. Ding, C. Yuan, S. Ai, M. Isakov, J. Wu, T. Wang, M. L. Dunn, H. J. Qi, *Sci Rep* **2016**, 6, 24761; b) Z. Zhao, X. Kuang, C. Yuan, H. J. Qi, D. Fang, *ACS Appl Mater Interfaces* **2018**, 10, 19932.

[11] a) C. P. Ambulo, J. J. Burroughs, J. M. Boothby, H. Kim, M. R. Shankar, T. H. Ware, *ACS Appl Mater Interfaces* **2017**, 9, 37332; b) E. C. Davidson, A. Kotikian, S. Li, J. Aizenberg, J. A. Lewis, *Adv Mater* **2020**, 32, e1905682; c) M. O. Saed, C. P. Ambulo, H. Kim, R. De, V. Raval, K. Searles, D. A. Siddiqui, J. M. O. Cue, M. C. Stefan, M. R. Shankar, T. H. Ware, *Advanced Functional Materials* **2019**, 29, 1806412.

[12] H. Yang, W. R. Leow, T. Wang, J. Wang, J. Yu, K. He, D. Qi, C. Wan, X. Chen, *Adv Mater* **2017**, 29, 1701627.

[13] S. E. Bakarich, R. Gorkin, 3rd, M. in het Panhuis, G. M. Spinks, *Macromol Rapid Commun* **2015**, 36, 1211.

[14] Y. F. Zhang, N. Zhang, H. Hingorani, N. Ding, D. Wang, C. Yuan, B. Zhang, G. Gu, Q. Ge, *Advanced Functional Materials* **2019**, 29.

[15] Q. Ge, C. K. Dunn, H. J. Qi, M. L. Dunn, *Smart Materials and Structures* **2014**, 23, 094007.

[16] G. Villar, A. D. Graham, H. Bayley, *Science* **2013**, 340, 48.

[17] a) R. Tao, L. Xi, W. Wu, Y. Li, B. Liao, L. Liu, J. Leng, D. Fang, *Composite Structures* **2020**, 252; b) C. Yang, M. Boorugu, A. Dopp, J. Ren, R. Martin, D. Han, W. Choi, H. Lee, *Materials Horizons* **2019**, 6, 1244.

[18] W. Zhang, H. Wang, H. Wang, J. Y. E. Chan, H. Liu, B. Zhang, Y. F. Zhang, K. Agarwal, X. Yang, A. S. Ranganath, H. Y. Low, Q. Ge, J. K. W. Yang, *Nat Commun* **2021**, 12, 112.

[19] a) J. E. M. Teoh, Y. Zhao, J. An, C. K. Chua, Y. Liu, *Smart Materials and Structures* **2017**, 26; b) S. Akbari, A. H. Sakhaei, K. Kowsari, B. Yang, A. Serjouei, Z. Yuanfang, Q. Ge, *Smart Materials and Structures* **2018**, 27.

[20] Q. Zhang, K. Zhang, G. Hu, *Sci Rep* **2016**, 6, 22431.

[21] a) M. Zarek, M. Layani, S. Eliazar, N. Mansour, I. Cooperstein, E. Shukrun, A. Szlar, D. Cohn, S. Magdassi, *Virtual and Physical Prototyping* **2016**, 11, 263; b) J. T. Miao, M. Ge, S. Peng, J. Zhong, Y. Li, Z. Weng, L. Wu, L. Zheng, *ACS Appl Mater Interfaces* **2019**, 11, 40642; c) B. Peng, Y. Yang, K. Gu, E. J. Amis, K. A. Cavicchi, *ACS Materials Letters* **2019**, 1, 410; d) Y. Y. C. Choong, S. Maleksaeedi, H. Eng, S. Yu, J. Wei, P.-C. Su, *Applied Materials Today* **2020**, 18.

[22] a) Y. Y. C. Choong, S. Maleksaeedi, H. Eng, P.-C. Su, J. Wei, *Virtual and Physical Prototyping* **2016**, 12, 77; b) Y. Y. C. Choong, S. Maleksaeedi, H. Eng, J. Wei, P.-C. Su, *Materials & Design* **2017**, 126, 219.

[23] W. Wang, J. Sun, B. Guo, X. Chen, K. P. Ananth, J. Bai, *Journal of the European Ceramic Society* **2020**, 40, 682.

[24] W. Voit, T. Ware, R. R. Dasari, P. Smith, L. Danz, D. Simon, S. Barlow, S. R. Marder, K. Gall, *Advanced Functional Materials* **2010**, 20, 162.

[25] a) J. Wu, Z. Zhao, C. M. Hamel, X. Mu, X. Kuang, Z. Guo, H. J. Qi, *Journal of the Mechanics and Physics of Solids* **2018**, 112, 25; b) H. Stutz, K. H. Illers, J. Mertes, *Journal of Polymer Science Part B: Polymer Physics* **1990**, 28, 1483; c) A. T. DiBenedetto, *Journal of Polymer Science Part B: Polymer Physics* **1987**, 25, 1949.

[26] J. Mattia, P. Painter, *Macromolecules* **2007**, 40, 1546.

[27] A. Kawasaki, J. Furukawa, T. Tsuruta, G. Wasai, T. Makimoto, *Die Makromolekulare Chemie: Macromolecular Chemistry and Physics* **1961**, 49, 76.

A mechanically robust and UV curable shape memory polymer (*t*BA-AUD SMP) system can be stretched by up to 1240% of its original length and is compatible with digital light processing (DLP)-based high-resolution 3D printing technology (up to 2 μm). The high deformability and fatigue resistance (more than 10,000 times loading-unloading) make *t*BA-AUD SMP an ideal 4D printing material for engineering applications.

Keyword: 4D printing, digital light processing, shape memory polymer, high stretchability

*Biao Zhang, Honggeng Li, Jianxiang Cheng, Haitao Ye, Amir Hosein Sakhaei, Chao Yuan, Ping Rao, Yuan-Fang Zhang, Zhe Chen, Rong Wang, Xiangnan He, Ji Liu, Rui Xiao, Shaoxing Qu, Qi Ge**

Title: Mechanically Robust and UV Curable Shape Memory Polymers for Digital Light Processing based 4D Printing

ToC figure

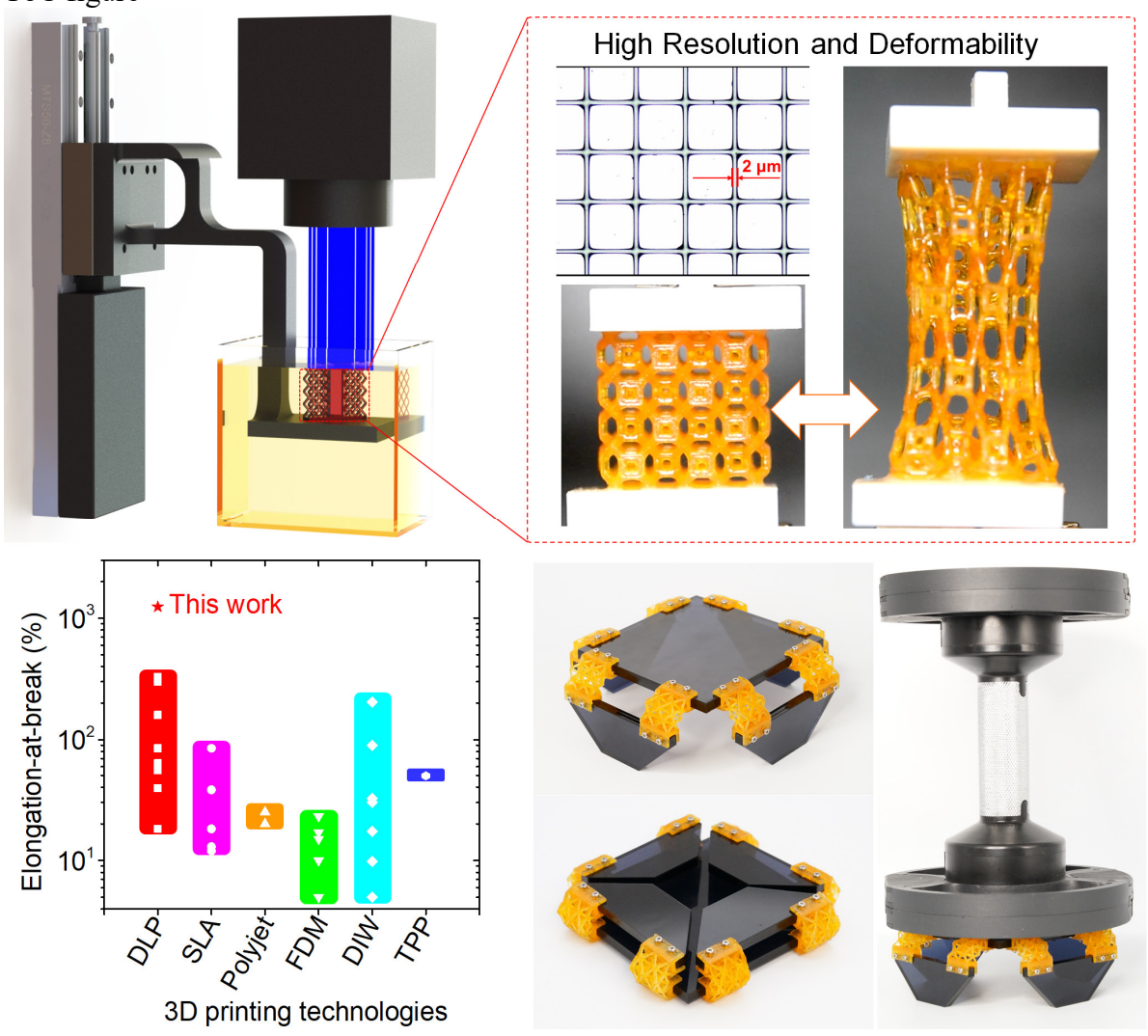

Supporting Information

Mechanically Robust and UV Curable Shape Memory Polymers for Digital Light Processing based 4D Printing

*Biao Zhang, Honggeng Li, Jianxiang Cheng, Haitao Ye, Amir Hosein Sakhaei, Chao Yuan, Ping Rao, Yuan-Fang Zhang, Zhe Chen, Rong Wang, Xiangnan He, Ji Liu, Rui Xiao, Shaoxing Qu, Qi Ge**

Prof. B. Zhang
Frontiers Science Center for Flexible Electronics (FSCFE), Xi'an Institute of Flexible Electronics (IFE) and Xi'an Institute of Biomedical Materials & Engineering (IBME), Northwestern Polytechnical University, 127 West Youyi Road, Xi'an 710072, China

Prof. B. Zhang, Dr. H. Li, J. Cheng, H. Ye., Prof. R. Wang, X. He, Prof. Ji Liu, Prof. Q. Ge
Shenzhen Key Laboratory of Biomimetic Robotics and Intelligent Systems, Department of Mechanical and Energy Engineering, Southern University of Science and Technology, Shenzhen, 518055, China
Guangdong Provincial Key Laboratory of Human-Augmentation and Rehabilitation Robotics in Universities, Southern University of Science and Technology, Shenzhen, 518055, China
E-mail: geq@sustech.edu.cn

Dr. A. H. Sakhaei
School of Engineering and Digital Arts,
University of Kent, Canterbury, Kent, CT2 7NT, United Kingdom

Prof. C. Yuan
State Key Laboratory for Strength and Vibration of Mechanical Structures, Department of Engineering Mechanics, Xi'an Jiaotong University, Xi'an 710049, China

Dr. P. Rao
Department of Mechanics and Aerospace Engineering,
Southern University of Science and Technology, Shenzhen, 518055, China

Dr. Y.-F. Zhang
Digital Manufacturing and Design Centre
Singapore University of Technology and Design, Singapore 487372, Singapore

Z. Chen, Prof. R. Xiao, Prof. S. Qu
State Key Laboratory of Fluid Power & Mechatronic System, Key Laboratory of Soft Machines and Smart Devices of Zhejiang Province, Department of Engineering Mechanics, Zhejiang University, Hangzhou 310027, China

B. Z., H. L., and J. C. contributed equally to this work.

Keywords: 4D printing, digital light processing, shape memory polymer, high stretchability

S1. Rheological characterizations

As shown in Figure S1, the concentration of the high molecular weight of the AUD crosslinker highly affects the rheological behavior of the *t*BA-AUD SMP precursor solutions. We performed the rheological characterizations to investigate the viscosity behavior of the *t*BA-AUD SMP precursor solutions. The tests were conducted on a Discovery Hybrid Rheometer (DHR2, TA instruments Inc., UK) with an aluminum plate geometry (40 mm in diameter, gap 500 μm). The tests were conducted with frequency ranging from 0.1 to 100 Hz. Figure S2 shows the viscosity of *t*BA-AUD SMP precursor solutions with the *t*BA/AUD ratios ranging from 0/10 to 10/0 as a function of shear rate.

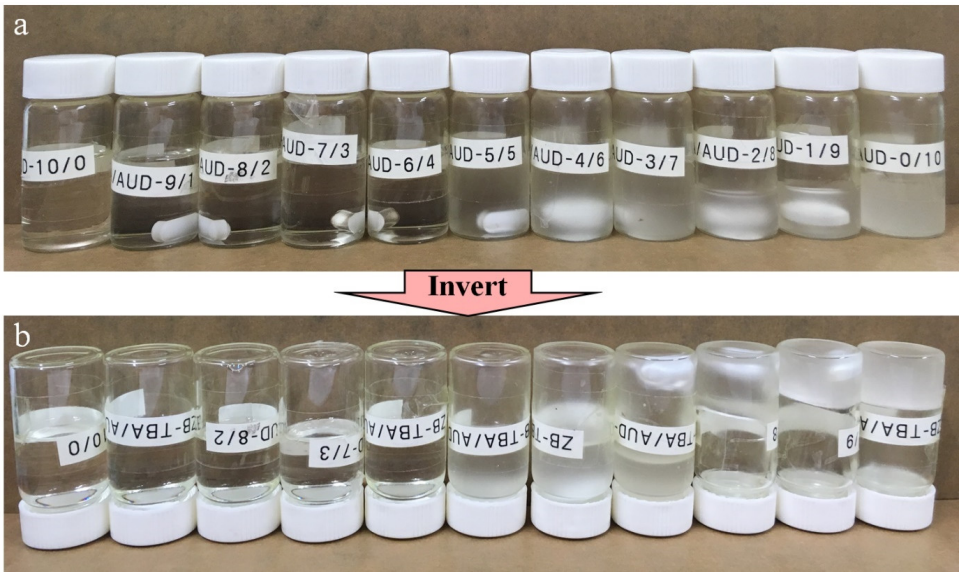

Figure S1. Images show (a) the prepared *t*BA-AUD SMP precursor solutions with the AUD content from 0 wt% to 100 wt% (from Left to Right) and the inversed vials demonstrating the effect of high viscosity of AUD on *t*BA-AUD SMP precursor solutions.

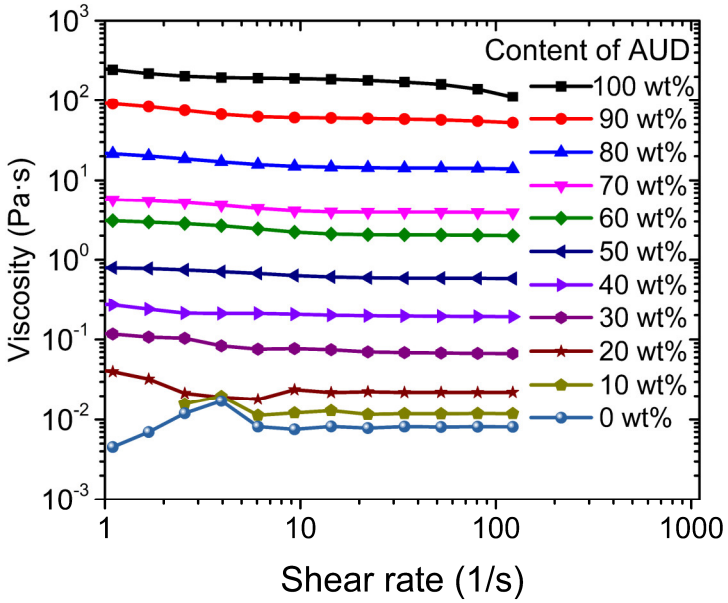

Figure S2. Rhelogical testing results on the *t*BA-AUD SMPs precursor solutions.

S2. Kinetic study of the *t*BA-AUD SMP system by the gel fraction characterizations

To study the kinetic behavior of *t*BA-AUD SMP system, a representative gel fraction with curing time relation to evaluate the kinetic behavior of a *t*BA-AUD SMP solution was measured, where the concentration of AUD is 50 wt%. We conducted the gel fraction tests by following the method reported by Gall and his coworkers.[1] We first prepared strip samples with weight of around 100 mg by curing them under 405 nm light source for 10 s, 20 s, 30 s, 60 s, 5 min and 10 min, respectively. Then, we placed the strip samples into the vials with approximately 20 mL of acetone where all the constituent materials of the *t*BA-AUD SMP are soluble. The vials were allowed to soak for one week to allow all noncrosslinked materials to be removed from the network polymer. The residues of strips were then removed from the acetone and placed in the oven at 60 °C for 24 h to drive off the remaining solvent. Then the obtained samples were exposed under air for 24 h. The weight of the final left polymer was measured and the gel fraction was calculated by the following equation:

$$\text{Gel fraction (\%)} = W_{\text{left}}/W_{\text{total}} \times 100\%.$$

Here, W_{total} represents the initial weight of the sample and W_{left} represents the weight of the final left polymer. Three samples of each polymer were measured to prove the repeatability. And the results were summaried in Figure S3.

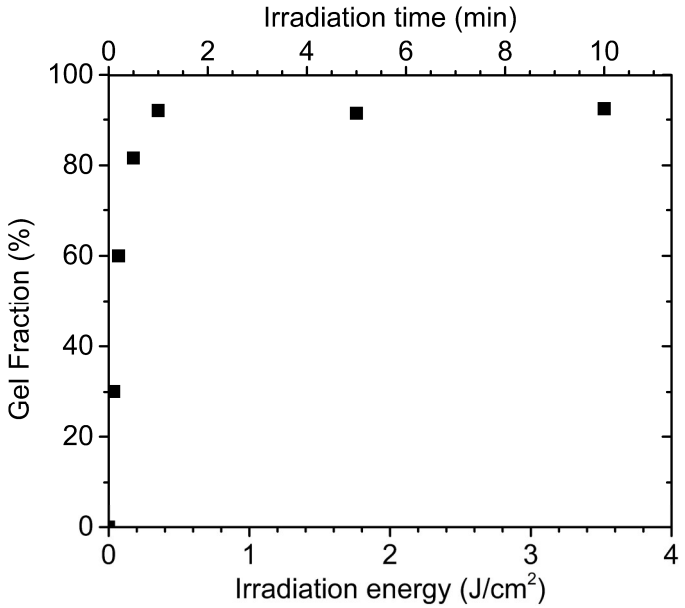

Figure S3. Gel fractions for a *t*BA-AUD SMPs resin (with 50% of AUD) with increasing irradiation energy and time.

S3. Dynamic mechanical analysis experiments

To study the thermomechanical properties of printed *t*BA-AUD SMP samples, dynamic mechanical analysis (DMA) was conducted with 3D printed *t*BA-AUD SMP samples that are printed using the resins with different AUD concentrations. Dynamic mechanical properties were studied by using a dynamic mechanical analysis (DMA) analyzer (Q800 DMA, TA Instruments) in the tension film mode. Samples for all the compositions were trimmed to a typical dimension of 15 mm × 5 mm × 1.0 mm and tested at a frequency of 1 Hz, a "force track" of 125% and an amplitude of 15 um. The temperature was first increased to 100 °C, held isothermally at 100 °C for 10 min to eliminate the thermal history. Then the temperature was cooled down at a heating rate of 2 °C/min. Figure S4 show the storage modulus and tanδ of *t*BA-AUD SMPs with different AUD concentration as a function of temperature, where storage

modulus corresponds to the elastic response of tested samples and tanδ is the ratio of loss modulus and storage modulus.

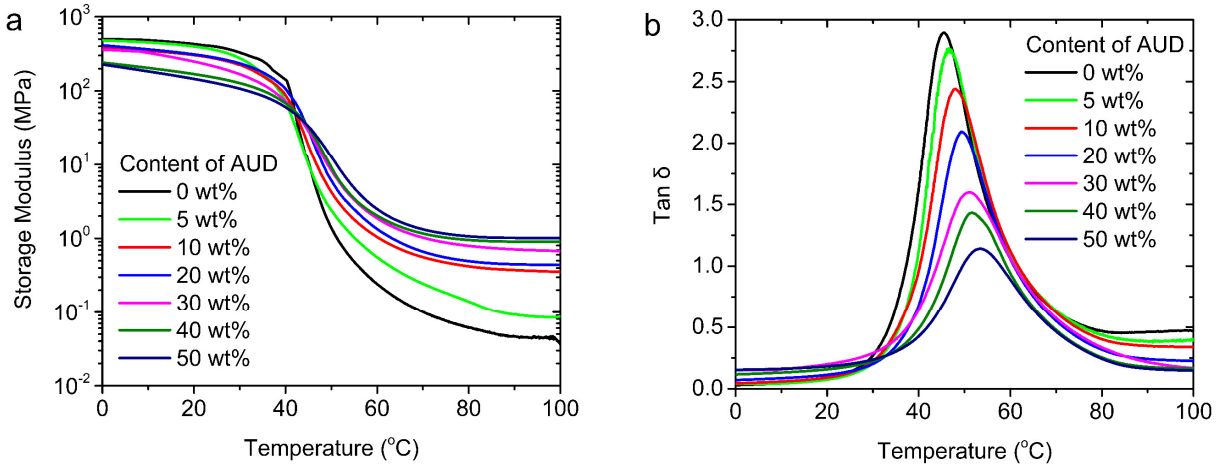

Figure S4. The thermomechanical properties of *t*BA-AUD SMPs with different AUD concentrations as a function of temperature.

S4. Uniaxial loading-unloading tests

We conducted the loading-unloading tests at the programming temperature (i.e. T_g+30 °C where the *t*BA-AUD SMP samples are at rubbery state) to investigate the effect of AUD content on the hysteresis behavior and residual strain. As shown in Figure S5a, the size of the hysteresis loop increases with the increase in the AUD content. Figure S5b clearly presents the residual strain with different AUD content. For the SMP sample with the AUD content less than 30 wt%, the residual strains are ~5%; the residual strains increase to 7.9% and 12.8% by increasing the AUD content to 40 wt% and 50 wt%, respectively.

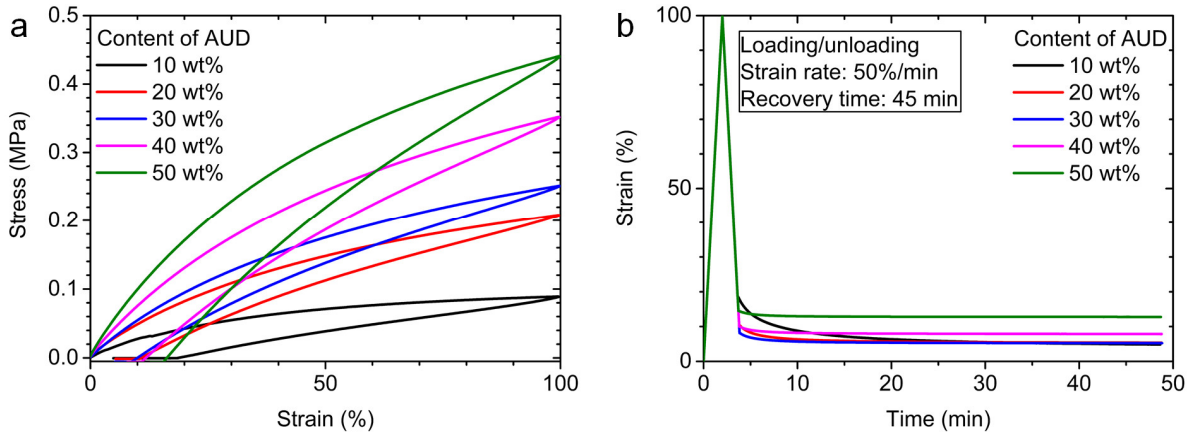

Figure S5. Uniaxial loading-unloading tests. (a) Stress-strain behavior. (b) Strain variation over time.

S5. Shape memory behavior tests

The shape memory (SM) behavior of the materials was investigated by following a typical shape memory cycling method. The sample was first stretched to 100% with a constant loading rate (6.00 %/min) at a programming temperature (i.e. T_g+30 °C), and then the temperature was decreased to room temperature (25 °C) with a cooling rate at 2 °C/min. After reached the target temperature, the sample was held isothermally for 2 min. By following the tensile was removed. In the free recovery step, the temperature was gradually increased to the recovery temperature (i.e. T_g+30 °C) at the rate of 2 °C/min. the sample was held isothermally for another 60 min. Figure S6 show the shape memory behavior of *t*BA-AUD SMPs with AUD content at 50 wt.%, 40 wt.%, 20 wt.%, and 10 wt.%, respectively.

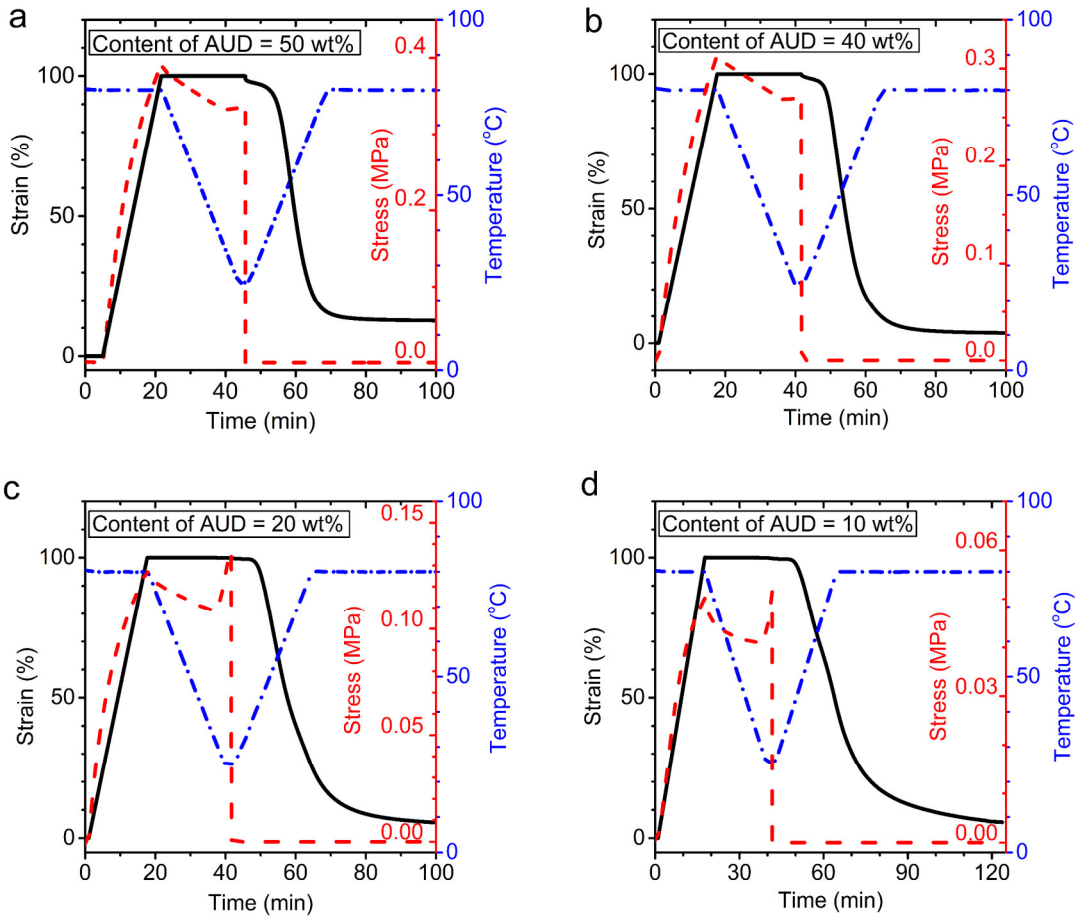

Figure S6. Shape memory behavior of *t*BA-AUD SMPs with AUD content at 50 wt.% (a), 40 wt.% (b), 20 wt.% (c), and 10 wt.% (d), respectively (R_f: shape fixity ratio; R_r: shape recovery ratio).

In addition, we conducted shape memory cyclic tests for the *t*BA-AUD with different AUD contents by stretching the samples to the 90% of elongation-at-break. As shown in Figure S7, all the SMP samples exhibit good shape memory behaviors even under extremely large deformations.

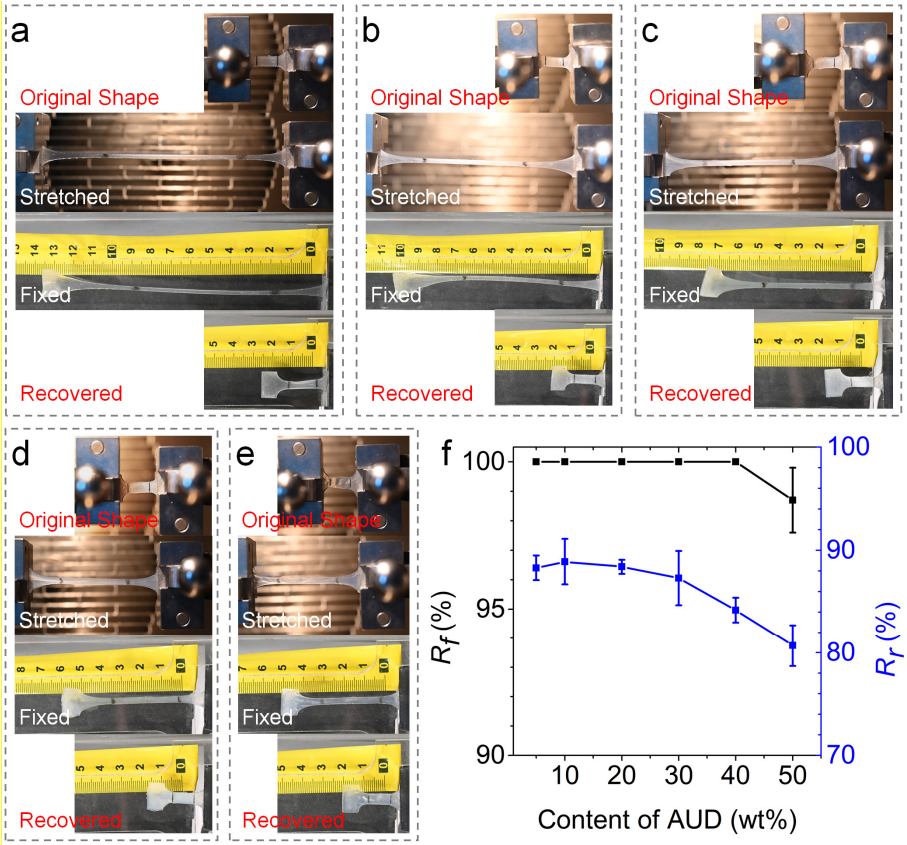

Figure S7. Shape memory behavior of the *t*BA-AUD SMP samples under large deformations. (a) SMP sample with 10 wt% AUD stretched by 810%; (b) SMP sample with 20 wt% AUD stretched by 540%; (c) SMP sample with 30 wt% AUD stretched by 360%; (d) SMP sample with 40 wt% AUD stretched by 270%; (e) SMP sample with 50 wt% AUD stretched by 240%; (f) Effects of AUD content on both shape fixity (R_f) and shape recovery ratio (R_r).

We further compare the shape memory behavior between the fresh SMP sample and the SMP sample after 10,000 cyclic loadings. Based on Figure 4g, after the 10,000 cyclic loading, the SMP with 10 wt% AUD can be only stretched by 470%. Therefore, in the shape memory cycle, we stretched both SMP samples by 300%. As shown in Figure S8, both samples have ~100% of shape fixity. However, about 40% residual strain still can be observed on the fresh SMP sample even after heating at 80 °C for 1 hour (Figure S8a). This is because that the hydrogen bonds exist in the fresh SMP sample, and the 300% strain leads to the breakage of hydrogen bonds as well as residual strain. In contrast, as shown in Figure S8b, the SMP sample after 10,000 cyclic loads is able to recover all the strain. This is because that the 10,000 cyclic loads

have broken all the hydrogen bonds, and there is no broken hydrogen bond as well as residual strain in the cyclically loaded SMP sample.

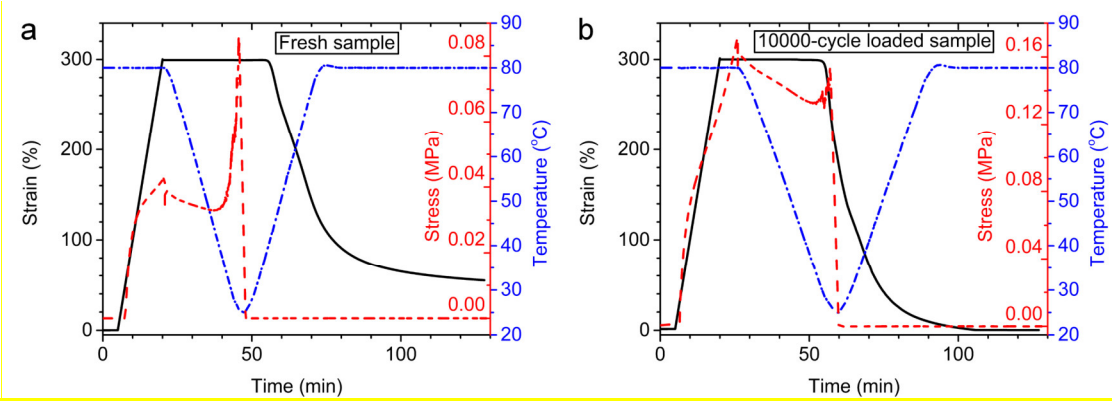

Figure S8. Comparison on the shape memory behaviors. (a) Fresh SMP sample. (b) SMP sample after 10,000 cyclic loadings.

S6. Fatigue tests

In order to evaluate the fatigue resistance of *Vero*, *t*BA-PEGDA SMP system and BMA-PEGDMA SMP system, the tensile fatigue tests were carried out using an ElectroForce machine (ET1-2, TA Instruments) at the corresponding rubbery state (i.e. T_g + 30 °C). All test samples are 20 mm × 5 mm × 2 mm (stretch section length is 10 mm) and at least three samples are to be tested for each sample. Firstly, the distance between the two clamps is set to 10 mm with the upper clamp holding the sample, and the lower clamp opens. The oven was then raised to 80 °C and kept for 5 minutes. Next, the sample was loaded and the cyclic tensile test was started. Figure S9, S10 and S11 show the fatigue testing results of *Vero*, *t*BA-PEGDA SMP system and BMA-PEGDMA SMP system, respectively.

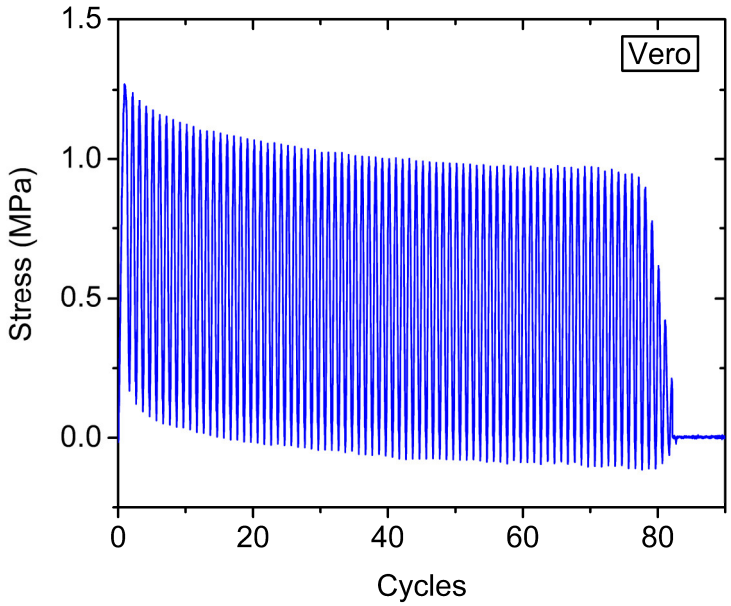

Figure S9. Fatigue test result of VeroClear at the rubbery state (i.e. 90 °C) with the strain between 10% - 20%.

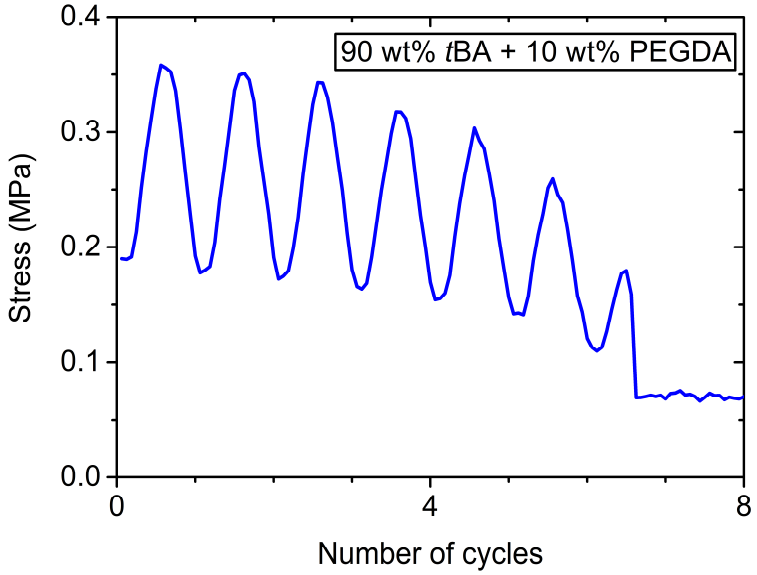

Figure S10. Fatigue test result of *t*BA-PEGDA (9:1, w/w) at the rubbery state (i.e. 74 °C) with the strain between 10% - 20%.

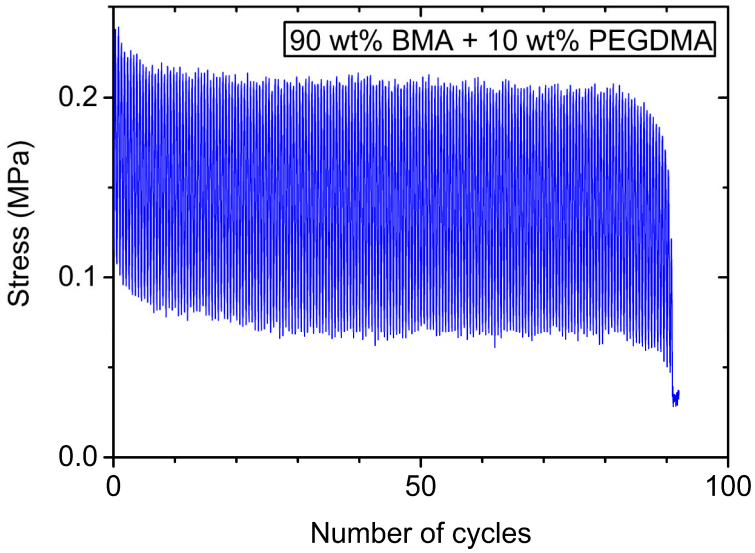

Figure S11. Fatigue test result of BMA-PEGDMA (9:1, w/w) at the rubbery state (i.e. 87 °C) with the strain between 20% - 40%.

S7. Uniaxial tensile testing results

To compare the break strains of *t*BA-AUD SMP system with *t*BA-PEGDA system, tension experiments on rectangular specimens of 3D printed *t*BA-PEGDA system samples with dimensions of 15 mm × 5 mm × 1.0 mm were conducted using MTS machine (100 N load cell, USA) with a thermal chamber at strain rate of 1%/s. The test temperature was set at higher temperature than T_g +30 °C of the corresponding specimen (*t*BA-PEGDA system). Uniaxial tensile test results were shown in Figure S12a. We further extracted data from Figure 3b and Figure S12a, and compared the elongation-at-break and Young's modulus relation between *t*BA-AUD system and *t*BA-PEGDA system. As shown Figure S12b, at the same Young's modulus (i.e., the same crosslinking density), the stretchability of the *t*BA-AUD SMP system is three to seven times higher than that of the *t*BA-PEGDA SMP system.

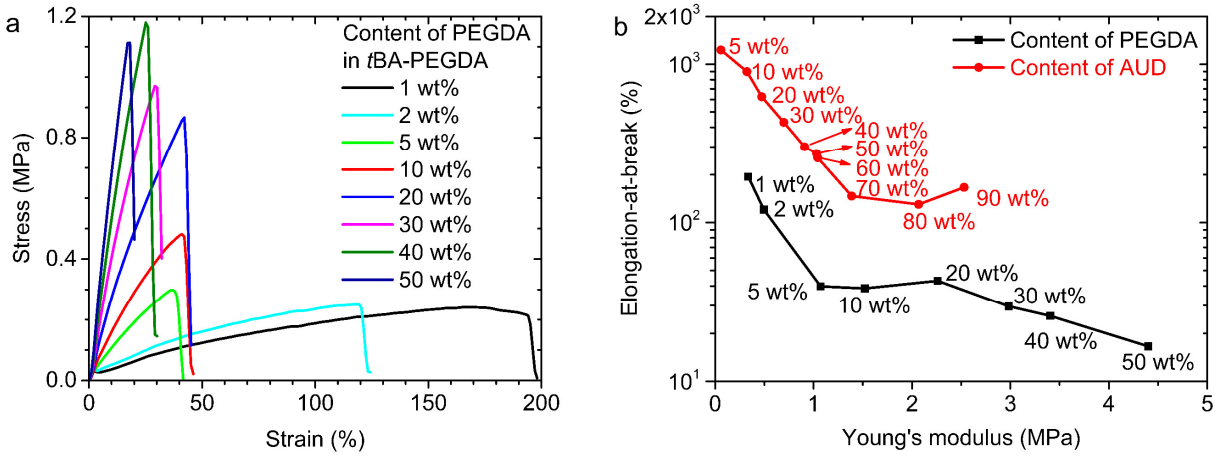

Figure S12. Uniaxial tensile test results. (a) Uniaxial tensile tests of the *t*BA-PEGDA SMP system at rubbery state. (b) Comparison on the elongation-at-break and Young's modulus relation between *t*BA-AUD system and *t*BA-PEGDA system.

S8. FTIR tests

To validate the existence of hydrogen bonds, we conducted FTIR tests. The Fourier transform infrared (FTIR) spectra were recorded using a FTIR spectrophotometer (Nicolet iS50 FT-IR Spectrometer, Thermo Scientific) in conjunction with platinum ATR single-reflection diamond accessory collecting 32 scans (resolution, 4 cm^{-1}) from 400 to 4000 cm^{-1}.

We first conducted the FTIR analysis on the sample made of pure *t*BA (i.e., Poly(*t*BA)) and AUD, respectively. As shown in the FTIR spectrum of Poly(*t*BA) (Figure S13), the stretching bands of the C-H aliphatic saturate at 2976, 2932 and 2850 cm^{-1}, the C=O group stretching is at 1724 cm^{-1}, the C-O-C group stretching is at 1141 cm^{-1}. The tertiary butyl group also gives two symmetrical methyl bending bands, and they are shown in the infrared spectrum of 2,2-dimethylheptane at 1392 and 1366 cm^{-1}. A weak band in the vicinity of 3430 cm^{-1} is assigned as the overtone of the C=O stretching band. Figure S13 also presents the FTIR spectrum of AUD where the stretching band of the N-H group is at 3384 cm^{-1}, the C-H aliphatic saturate at 2949, 2867 and 2796 cm^{-1}, the C=O stretching is at 1720 cm^{-1}, the C-O-C stretching is at 1182 cm^{-1}, the C=C stretching is at 810 and 1405 cm^{-1}, the -CH_2- stretching is at 1254 cm^{-1} and C-N stretching is at 1236 cm^{-1}.

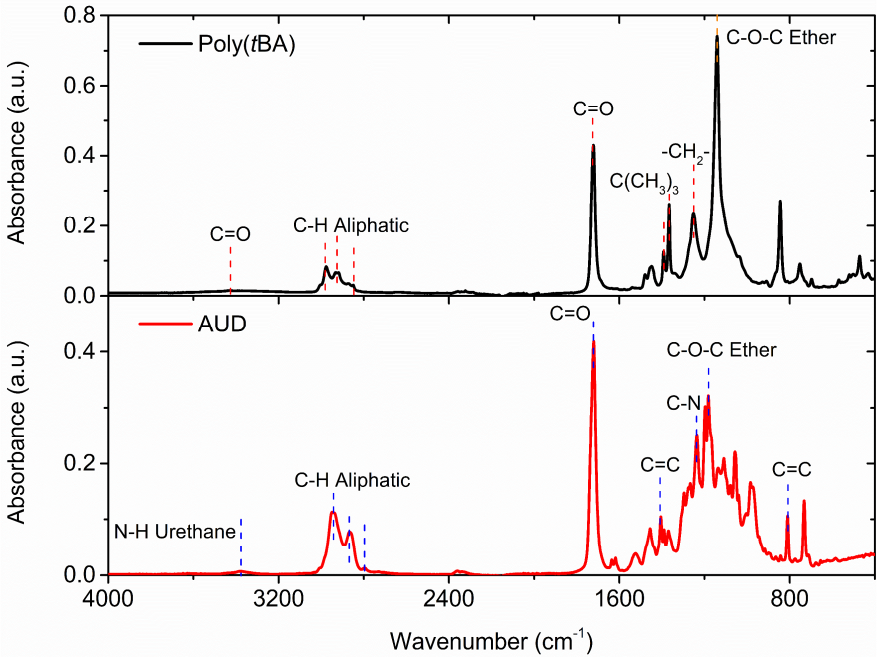

Figure S13. FTIR spectra of Poly(*t*BA) and AUD.

As FTIR spectroscopy is highly sensitive to hydrogen bonding,[2] the formed hydrogen bonds between the C=O and N-H groups (Figure S14) in *t*BA-AUD SMP system could be identified from the C=O and N-H stretching vibrations near 1600-1800 cm^{-1} and 3200-3400 cm^{-1}, respectively.

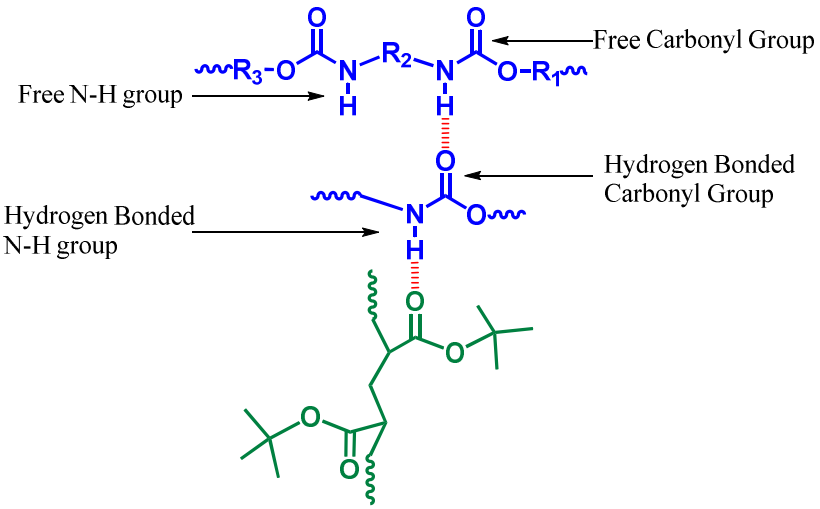

Figure S14. Band assignments for the C=O and N-H stretching modes in the *t*BA-AUD SMP.

To validate the presence of hydrogen bonds, we performed Fourier Transformation Infrared Spectroscopy (FTIR) tests (Figure S13, Figures 4c and d). As shown in Figure 4c, the C=O group stretching of the pure *t*BA sample (AUD content: 0 wt%) is at 1724 cm^{-1}, and the increase in the AUD content shifts the C=O group stretching to lower wavenumber due to the presence of hydrogen bonds between the C=O and N-H groups (Figure S14).[2] More importantly, the 10,000-cycle fatigue loading makes the C=O peak shape become narrow and slightly shift to the left. Moreover, from the wavenumber range from 3200-3400 cm^{-1} in Figure 4d, we could only observe the overtone stretching of the C=O group at 3430 cm^{-1} from the pure *t*BA sample,[3] and the stretching of the N-H group at 3384 cm^{-1} from the pure AUD sample; from the *t*BA-AUD SMP samples, we can observe both the stretching bands, but the stretching of the C=O group becomes broader, and the stretching of the N-H group shifts to lower wavenumber due to the presence of hydrogen bonds. Again, the fatigue cyclic loading weakens vibration peaks located at 3384 cm^{-1} and 3430 cm^{-1}.

In addition, we could also validate the existence of hydrogen bonds by comparing the Amide III (C-N) bands from the FTIR spectrum [4]. As shown in Figure S15, for the pure *t*BA sample, only one band belonging to the -CH_2- group vibration is found at 1254 cm^{-1} in the 1320-1220 cm^{-1} region. When the AUD content increases to 10 wt%, we observe new broad peaks at 1302 and 1240 cm^{-1} ascribed to the stretching of C-N vibration. Once the AUD content increases to 100 wt%, the two peaks shift to lower wavenumbers which can be explained by the increase in hydrogen bonds. Moreover, after 10,000-cycle fatigue, the peak at 1302 cm^{-1} disappears, and a narrow peak at 1253 cm^{-1} is found. This can be attributed to the breakage of hydrogen bonds.

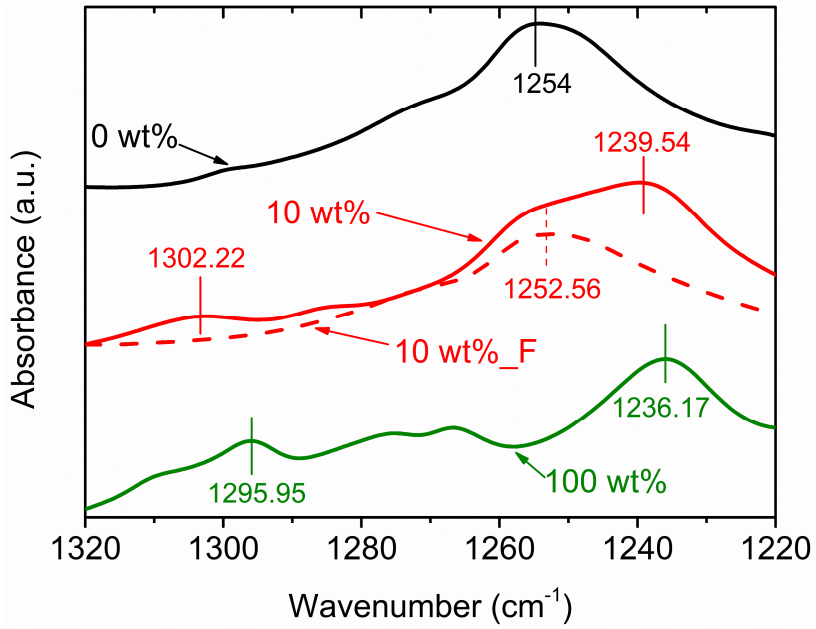

Figure S15. FTIR spectrum at the ranges of 1220-1320 cm^{-1}.

S9. Comparison of 3D printing shape memory polymers

To compare the properties of other shape memory systems with our *t*BA-AUD SMP system, we carried out the dynamic mechanical analysis and uniaxial tensile tests. The results were shown as follows:

The AA-BPA SMP system was reported by Lee and coworkers (Details can be seen in Table S1). The samples were prepared by obeying the related literature. The photo-curable SMP precursor solution was prepared by mixing acrylic Acid (AA) and Bisphenol A ethoxylate dimethacrylate (BPA) (M_n = 1700) at a ratio of 55:45 in weight. Phenylbis(2,4,6-trimethylbenzoyl) phosphine was added at the concentration of 2 wt% of the precursor solution as photoinitiator. The resulting samples from the precursor solution were characterized and shown in Figure S16 and S17, respectively.

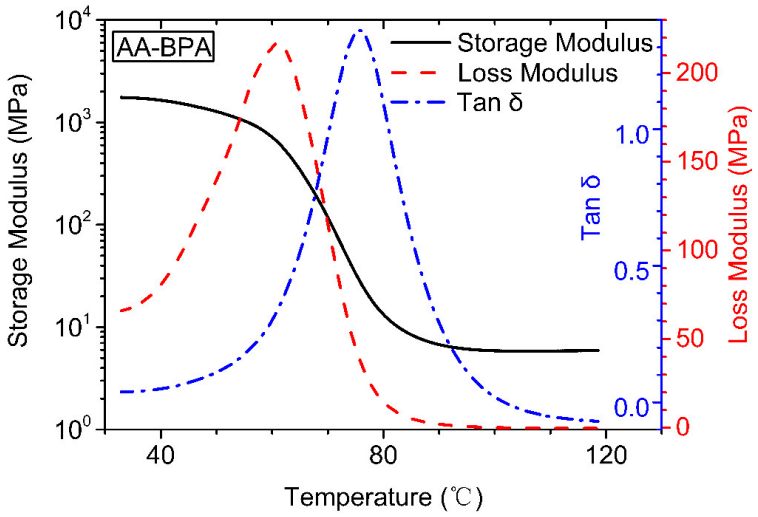

Figure S16. Storage modulus, loss modulus and tan δ of the AA-BPA SMP. (The DMA experiment was conducted on a dynamic mechanical analyzer (Q800, TA Instruments) using a tensile loading mode. Dimensions of 3D printed samples were 25 mm × 8 mm × 1 mm. Specimens were heated in a temperature oven at 120 ℃ for 12 hours to remove moisture absorbed and kept in a dry box with desiccants. Testing parameters for DMA included strain of 0.2 %, frequency of 1 Hz, preload of 0.001 N, and force track of 150 %. Specimens were heated at 30 ℃ for 10 min prior to each test. Storage modulus, loss modulus, and tan δ were measured as a function of temperature while temperature was increased to 120 ℃ at a rate of 1 ℃ min^{-1}).

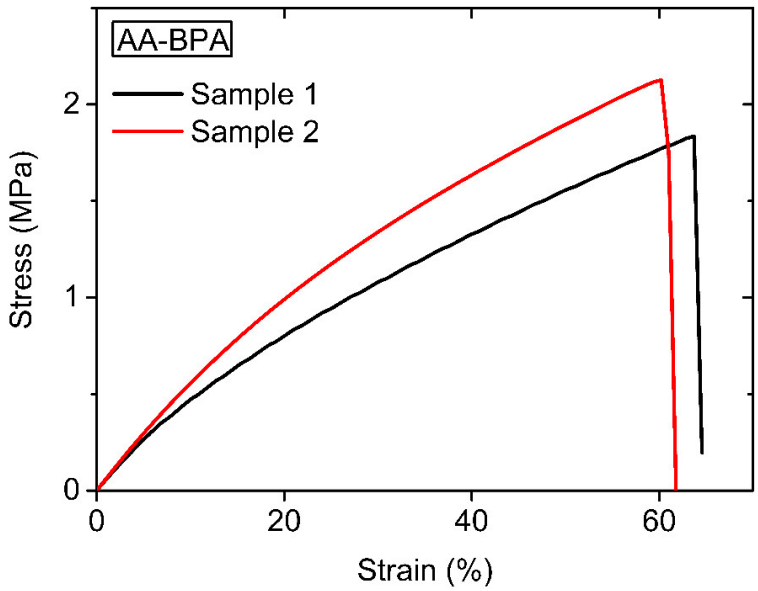

Figure S17. Uniaxial tensile test results of AA-BPA SMP at the rubbery state (tension experiments on rectangular specimens of AA-BPA SMP with dimensions of 15 mm × 5 mm × 1.0 mm were conducted using ynamic mechanical analyzer (Q800, TA Instruments) at strain rate of 1%/s. The test temperature was set at higher temperature than T_g +30 °C of the corresponding specimen (i.e. 100 °C)).

Polylactic Acid (PLA) and PLA based composites have been widely used as SMP in FDM and DIW based 3D printing (Details can be seen in Table S1). The mechnical performance of 3D printed PLA samples (JG AURORA, China) were characterized, and the results were shown in Figure S18, S19 and S20, respectively.

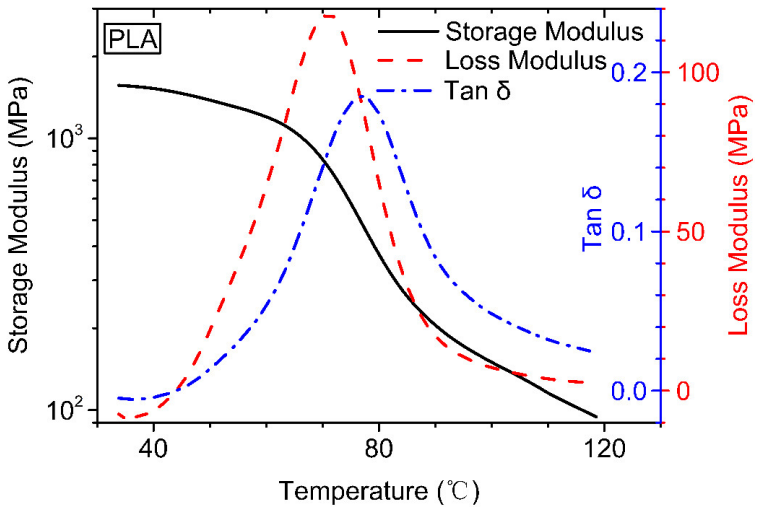

Figure S18. Storage modulus, loss modulus and tan δ of the PLA. (The DMA experiment was conducted on a dynamic mechanical analyzer (Q800, TA Instruments) using a tensile loading mode. Dimensions of 3D printed samples were 25 mm × 8 mm × 1 mm. Specimens were heated in a temperature oven at 120 ℃ for 12 hours to remove moisture absorbed and kept in a dry box with desiccants. Testing parameters for DMA included strain of 0.2 %, frequency of 1 Hz, preload of 0.001 N, and force track of 150 %. Specimens were heated at 30 ℃ for 10 min prior to each test. Storage modulus, loss modulus, and tanδ were measured as a function of temperature while temperature was increased to 120 ℃ at a rate of 1 ℃/min).

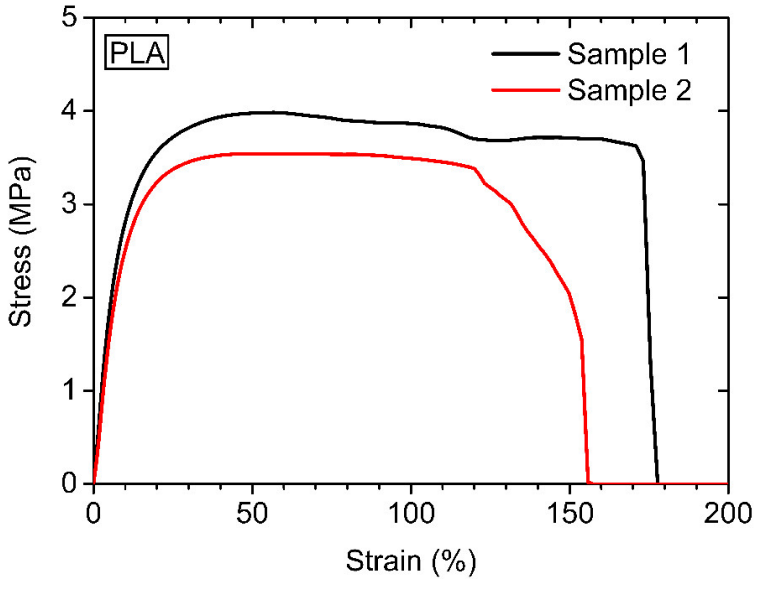

Figure S19. Uniaxial tensile test results of PLA at the rubbery state (tension experiments on rectangular specimens of PLA with dimensions of 15 mm × 5 mm × 1.0 mm were conducted using dynamic mechanical analyzer (Q800, TA Instruments) at strain rate of 1%/s. The test temperature was set at higher temperature than T_g +30 °C of the corresponding specimen (i.e. 110 °C)).

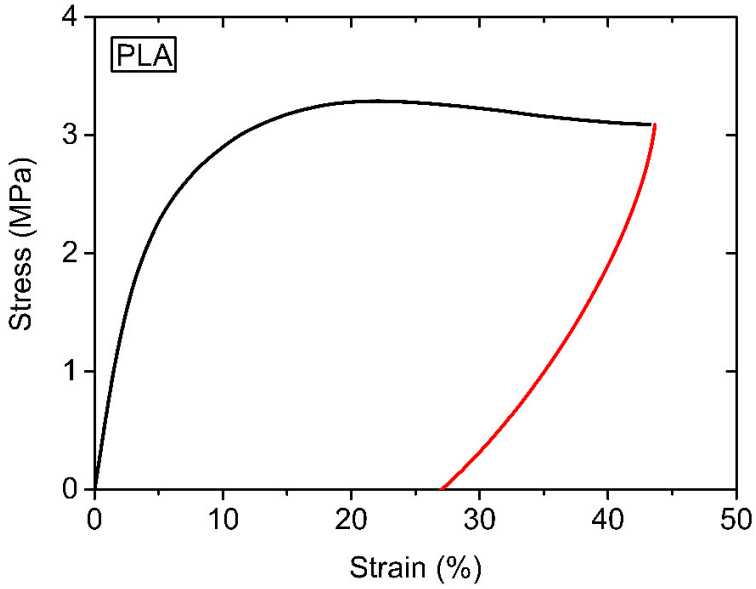

Figure S20 Loading-unloading cyclic test of PLA at 110 °C. (Using Dynamic mechanical analysis (DMA, Q800 DMA, TA Instruments), 45% strain was stretched at 110 °C at a strain rate of 10%/min. Then, the stress is unloaded at the same rate. The sample was trimmed to a size of 15 mm × 5 mm × 0.5 mm).

S10. Uniaxial tensile test results of *t*BA-AUD SMPs at room temperature

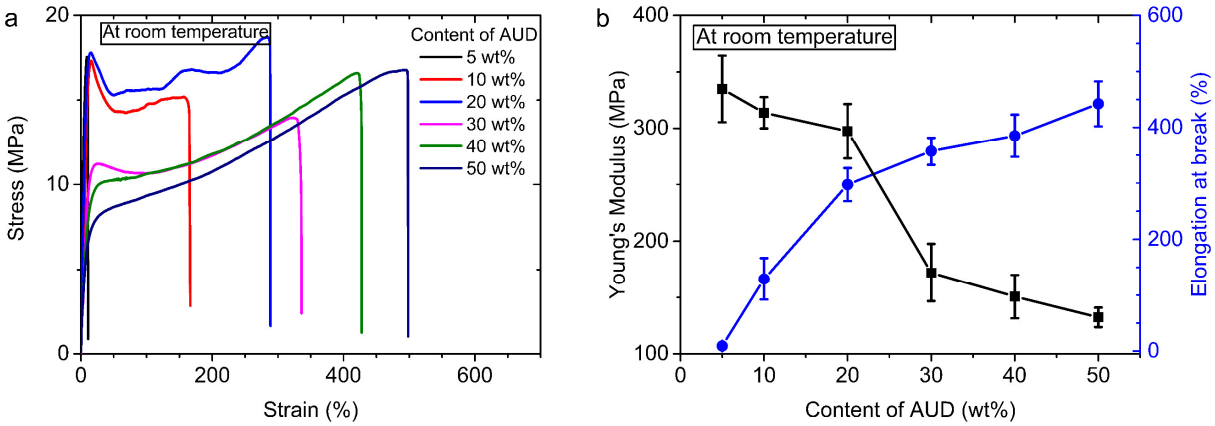

Figure S21. Uniaxial tensile test results of TBA-AUD SMP system with different ratios at room temperature (i.e. 20 °C). (a) stress strain behavior. (b) The relation between Young's Modulus and AUD content as well as the relation between elongation-at-break and AUD content.

Table S1. Summary of 3D printing shape memory polymers.

Technique	Material	Specified resolution [μm]	Glass Transition temperature/T_g [ºC]	Break strain [%]	Curing time [s]	Reference
DLP	BMA/DEGDMA/PEGDMA/BPA	30	30 - 180	100-330 (Er)	~ 60	[5]
DLP	PCLDMA/UPyMA	85	55	230- 300 (<Tm)	~20	[6]
DLP	PCLDMA	39	43-51(Tm)	4-55	10 - 50	[7]
DLP	IBOMA/Cubiflow	-	112	82	40 (50 μm)	[8]
DLP	PCLDMA	39	55(Tm)	<160 (Em)	9	[9]
DLP	PCLDMA	39 or 50	40 -50 (Tm)	~330%	9	[10]
DLP (PμSL)	AA/BPA	13	71	~64	5 (50 μm)	[11]
DLP	MEFB/IBOA/EGPEA/HPASi	25	57-70	39.3	10.8 (100 μm)	[12]
DLP	EHA/IBoA/PEGDMA/VBTOP-SS	50	61, 152	-	15s (80 μm)	[13]
DLP/SLA	*t*BA/DEGDA	39	53.9-74.1	<18.2	1-40 (0-1509 μm)	[14]
DLP/SLA	*t*BA/DEGDA/nanosilica	39	37.8-62.6	10-85	7s	[15]
SLA	PP-DGEBA/DGEBHA/OXT/ DGEDA/EO3-TMPTA	50-100	82	38	-	[16]
SLA	PUA/IBOA/DGEDA	- -	92	~85 (70 ºC)	-	[17]
SLA	Clear FLGPCL02	140	58.4	12	-	[18]
SLA	SOEA	190	20	45-90°	40mm/s	[19]
SLA	Accura® 60	50, 100	58	5~13	30	[20]
Polyjet	Vero	50-200	~58	10-25	1~2	[21]
Polyjet	TangoBlackPlus/Verowhite Plus	200	47.4-55.6	10-25	1~2	[22]
Polyjet	VeroClear	50	2~58	20	1~2	[23]
FDM	PU/CB	800	29.3 – 40.5	0-180º	-	[24]
FDM	SEBS/PE	400	50-95	180°	-	[25]
FDM	PLA/Fe_3O_4	400	65-67	<17	5mm/min	[26]
FDM	PLA/CNT	400	65-67	~5	5mm/min	[27]

FDM	PLA/TPU	200	~70	<10	10mm/s	[28]
FDM	PLA	100	60~65	13~23	10-150 mm/s	[29]
FDM	PLA	400	60	-	20,40,70 mm/s	[30]
FDM	PLA/PHA/wood fibres	400	-	1-5	1-5 mm/s	[31]
FDM	PLA/Fe_3O_4	500	62.7-66.7	-	2mm/min	[32]
FDM	PLA/HA	350	53.5	15	30mm/s	[33]
FDM	TPU	400	35	-	40mm/s	[34]
FDM	PVA05, PVA05GLY	400	57,11	-	23mm/s	[35]
DIW	PLA/c-PLA/ F_3O_4	100,150, 200,510	48,53,61	32.4,60.8, 203.5	0.4-2mm/s	[36]
DIW	PLMC copolymers	160,200, 260	50.16, 65.14	9.8-30	1-9mm/s	[37]
DIW	PLMC/CNT nanocomposites	200	65-69	40-90	0.5mm/s	[38]
DIW (SC)	Ag@CNF/PLA/DCM	200	~80.5	17.3-2	0.2-10mm/s	[39]
TPP	HPPA/BPA/Vero	0.3	~40	~50	1.1 mm/s	[40]

Note: BMA: Benzyl Methacrylate; DEGDMA: Di(ethylene glycol) Dimethacrylate; PEGDMA: Poly(ethylene glycol) Dimethacrylate; BPA: Bisphenol A ethoxylate dimethacrylate; PCLDMA: Polycaprolactone dimethacrylate; UpyMA: Methacrylates bearing 2-ureido-4[2H]-pyrimidinone motifs; IBOMA: Isobornyl methacrylate; Cubiflow: a commercial available 3D printing resin based on IBOMA and difunctional methacryaltes; AA: acrylic acid; BPA: Bisphenol A ethoxylate dimethacrylate; IBOA: Isobornyl acrylate; EGPEA: Ethylene glycol phenyl ether acrylate; MEFB: 2-(Methacryloyloxy)ethyl 4-formylbenzoate; HPASi: Hyperbranched polysiloxane; EHA 2-Ethylhexyl acrylate; VBTOP-SS: viniylbenzyltrio ctylphosphonium 4-styrenesulfonate; tBA: *tert*-Butyl acrylate; DEGDA: Di(ethylene glycol) diacrylate; DGEBA: Diglycidyl ether of bisphenol A; DGEHBA: Diglycidyl ehter of hydrogenated bisphenol A; OXT: 30ethyl-3-hydroxymethyl oxetane; DGEDA: Bisphenol A diglycidyl ehter diacrylate; EO_3-TMPTA: Ethylene oxide modified trimethylol propane triacrylate; PUA: Polyurethane acrylate; Clear FLGPCL02: A photopolymer resin from Formlabs company; SOEA: Soybean oil epoxidized acrylate; Accura® 60: A commercial available epoxy resin from 3D system; Vero and Tango: Commercial photopolymer resins from Stratasys; PU: polyurethane; CB: Carbon Black; SEBS: a kind of typical triblock co-polymer consisting of polystyrene (PS) microdomains and a poly-ethylene-co-butylene (EB) matrix; PE: polyethylene; PLA: Polylactic Acid; CNT: Carbon nanotube; TPU: Thermoplastic polyurethane; PVA: Polyvinyl alcohol; PLMC: Poly(d, l-lactide-co-trimethylene carbonate); BP: Benzophenone; SC printing: Solvent casting printing; CNF: Carbon nanofibers; DCM: Dichloromethance; PCL: Polycaprolactone; PHA: Poly(hydroxyalkanoate); HA: hydroxyapatite; HPPA: 2-hydroxy-3-phenoxypropyl acrylate.

References

[1] W. Voit, T. Ware, R. R. Dasari, P. Smith, L. Danz, D. Simon, S. Barlow, S. R. Marder, K. Gall, *Advanced Functional Materials* **2010**, 20, 162.

[2] a) J. Mattia, P. Painter, *Macromolecules* **2007**, 40, 1546; b) D. K. Patel, A. H. Sakhaei, M. Layani, B. Zhang, Q. Ge, S. Magdassi, *Adv Mater* **2017**, 29, 1606000.

[3] A. Kawasaki, J. Furukawa, T. Tsuruta, G. Wasai, T. Makimoto, *Die Makromolekulare Chemie: Macromolecular Chemistry and Physics* **1961**, 49, 76.

[4] a) G. Suchkova, L. Maklakov, Vibrational Spectroscopy **2009**, 51, 333; b) W. Herrebout, K. Clou, H. Desseyn, The Journal of Physical Chemistry A **2001**, 105, 4865; c) K. Nakayama, T. Ino, I. Matsubara, Journal of Macromolecular Science—Chemistry **1969**, 3, 1005.

[5] Q. Ge, A. H. Sakhaei, H. Lee, C. K. Dunn, N. X. Fang, M. L. Dunn, *Sci Rep* **2016**, 6, 31110.

[6] M. Invernizzi, S. Turri, M. Levi, R. Suriano, *European Polymer Journal* **2018**, 101, 169.

[7] M. Zarek, M. Layani, S. Eliazar, N. Mansour, I. Cooperstein, E. Shukrun, A. Szlar, D. Cohn, S. Magdassi, *Virtual and Physical Prototyping* **2016**, 11, 263.

[8] B. Steyrer, P. Neubauer, R. Liska, J. Stampfl, *Materials (Basel)* **2017**, 10.

[9] M. Zarek, M. Layani, I. Cooperstein, E. Sachyani, D. Cohn, S. Magdassi, *Adv Mater* **2016**, 28, 4449.

[10] M. Zarek, N. Mansour, S. Shapira, D. Cohn, *Macromol Rapid Commun* **2017**, 38.

[11] C. Yang, M. Boorugu, A. Dopp, J. Ren, R. Martin, D. Han, W. Choi, H. Lee, *Materials Horizons* **2019**, 6, 1244.

[12] J. T. Miao, M. Ge, S. Peng, J. Zhong, Y. Li, Z. Weng, L. Wu, L. Zheng, *ACS Appl Mater Interfaces* **2019**, 11, 40642.

[13] B. Peng, Y. Yang, K. Gu, E. J. Amis, K. A. Cavicchi, *ACS Materials Letters* **2019**, 1, 410.

[14] a) Y. Y. C. Choong, S. Maleksaeedi, H. Eng, P.-C. Su, J. Wei, *Virtual and Physical Prototyping* **2016**, 12, 77; b) Y. Y. C. Choong, S. Maleksaeedi, H. Eng, J. Wei, P.-C. Su, *Materials & Design* **2017**, 126, 219.

[15] Y. Y. C. Choong, S. Maleksaeedi, H. Eng, S. Yu, J. Wei, P.-C. Su, *Applied Materials Today* **2020**, 18.

[16] H. Yang, W. R. Leow, T. Wang, J. Wang, J. Yu, K. He, D. Qi, C. Wan, X. Chen, *Adv Mater* **2017**, 29, 1701627.

[17] T. Zhao, R. Yu, X. Li, B. Cheng, Y. Zhang, X. Yang, X. Zhao, Y. Zhao, W. Huang, *European Polymer Journal* **2018**, 101, 120.

[18] a) S. Pandini, N. Inverardi, G. Scalet, D. Battini, F. Bignotti, S. Marconi, F. Auricchio, *Mechanics Research Communications* **2020**, 103; b) N. Inverardi, S. Pandini, F. Bignotti, G. Scalet, S. Marconi, F. Auricchio, *Macromolecular Materials and Engineering* **2019**, 305.

[19] S. Miao, H. Cui, M. Nowicki, L. Xia, X. Zhou, S. J. Lee, W. Zhu, K. Sarkar, Z. Zhang, L. G. Zhang, *Adv Biosyst* **2018**, 2.

[20] A. D. Lantada, A. de Blas Romero, E. C. Tanarro, *Smart Materials and Structures* **2016**, 25.

[21] Z. Ding, C. Yuan, X. Peng, T. Wang, H. J. Qi, M. L. Dunn, *Sci Adv* **2017**, 3, e1602890.

[22] J. E. M. Teoh, Y. Zhao, J. An, C. K. Chua, Y. Liu, *Smart Materials and Structures* **2017**, 26.

[23] S. Akbari, A. H. Sakhaei, K. Kowsari, B. Yang, A. Serjouei, Z. Yuanfang, Q. Ge, *Smart Materials and Structures* **2018**, 27.

[24] H. Yang, W. R. Leow, T. Wang, J. Wang, J. Yu, K. He, D. Qi, C. Wan, X. Chen, *Adv Mater* **2017**, 29.

[25] S. Chen, Q. Zhang, J. Feng, *Journal of Materials Chemistry C* **2017**, 5, 8361.
[26] C. Lin, J. Lv, Y. Li, F. Zhang, J. Li, Y. Liu, L. Liu, J. Leng, *Advanced Functional Materials* **2019**, 29.
[27] Y. Liu, W. Zhang, F. Zhang, J. Leng, S. Pei, L. Wang, X. Jia, C. Cotton, B. Sun, T.-W. Chou, *Composites Science and Technology* **2019**, 181.
[28] M. Carlson, Y. Li, *The International Journal of Advanced Manufacturing Technology* **2020**, 106, 4263.
[29] Q. Zhang, D. Yan, K. Zhang, G. Hu, *Sci Rep* **2015**, 5, 8936.
[30] a) M. Bodaghi, R. Noroozi, A. Zolfagharian, M. Fotouhi, S. Norouzi, *Materials (Basel)* **2019**, 12; b) Q. Zhang, K. Zhang, G. Hu, *Sci Rep* **2016**, 6, 22431.
[31] A. Le Duigou, M. Castro, R. Bevan, N. Martin, *Materials & Design* **2016**, 96, 106.
[32] F. Zhang, L. Wang, Z. Zheng, Y. Liu, J. Leng, *Composites Part A: Applied Science and Manufacturing* **2019**, 125.
[33] a) F. S. Senatov, K. V. Niaza, M. Y. Zadorozhnyy, A. V. Maksimkin, S. D. Kaloshkin, Y. Z. Estrin, *J Mech Behav Biomed Mater* **2016**, 57, 139; b) F. S. Senatov, M. Y. Zadorozhnyy, K. V. Niaza, V. V. Medvedev, S. D. Kaloshkin, N. Y. Anisimova, M. V. Kiselevskiy, K.-C. Yang, *European Polymer Journal* **2017**, 93, 222.
[34] S. T. Ly, J. Y. Kim, *International Journal of Precision Engineering and Manufacturing-Green Technology* **2017**, 4, 267.
[35] A. Melocchi, N. Inverardi, M. Uboldi, F. Baldi, A. Maroni, S. Pandini, F. Briatico-Vangosa, L. Zema, A. Gazzaniga, *Int J Pharm* **2019**, 559, 299.
[36] H. Wei, Q. Zhang, Y. Yao, L. Liu, Y. Liu, J. Leng, *ACS Appl Mater Interfaces* **2017**, 9, 876.
[37] X. Wan, H. Wei, F. Zhang, Y. Liu, J. Leng, *Journal of Applied Polymer Science* **2019**, 136.
[38] X. Kuang, D. J. Roach, J. Wu, C. M. Hamel, Z. Ding, T. Wang, M. L. Dunn, H. J. Qi, *Advanced Functional Materials* **2019**, 29, 1805290.
[39] H. Wei, X. Cauchy, I. O. Navas, Y. Abderrafai, K. Chizari, U. Sundararaj, Y. Liu, J. Leng, D. Therriault, *ACS Appl Mater Interfaces* **2019**, 11, 24523.
[40] W. Zhang, H. Wang, H. Wang, J. Y. E. Chan, H. Liu, B. Zhang, Y.-F. Zhang, K. Agarwal, X. Yang, A. S. Ranganath, H. Y. Low, Q. Ge, J. K. W. Yang, Nature Communications **2021**, 12. 112.

List of Movies:

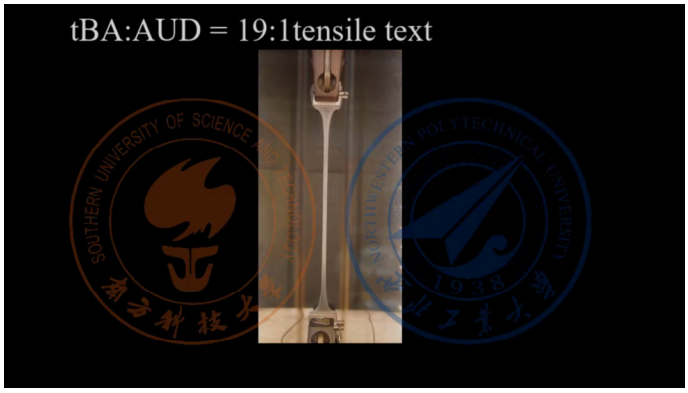

Movie S1. Stretching a *t*BA-AUD SMP sample with 5 wt.% AUD at 80 ℃.

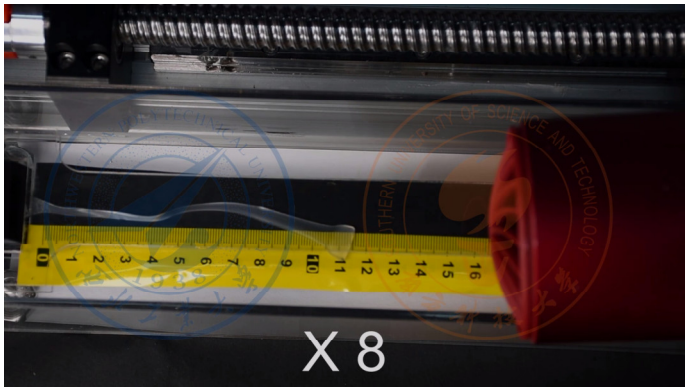

Movie S2. Recovery of a *t*BA-AUD SMP sample which was stretched by 1240%.

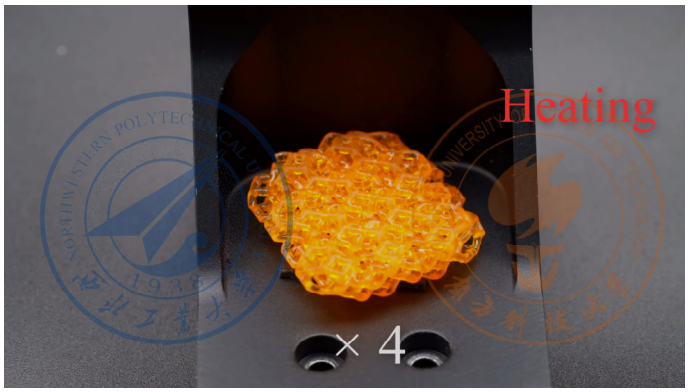

Movie S3. Recovery of a compressed 4D printed Kelvin form upon heating.

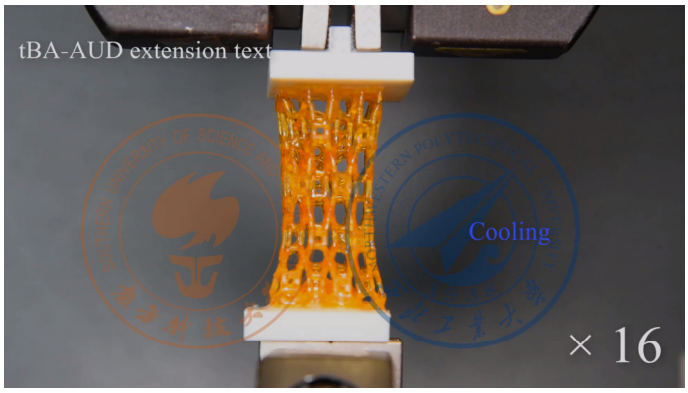

Movie S4. Shape memory process of a 4D printed Kelvin form under extension.

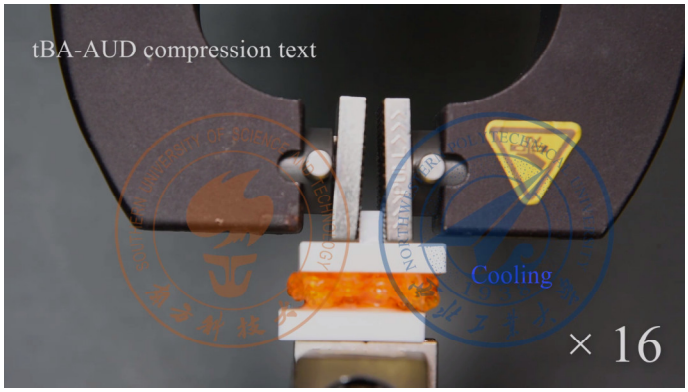

Movie S5. Shape memory process of a 4D printed Kelvin form under compression.

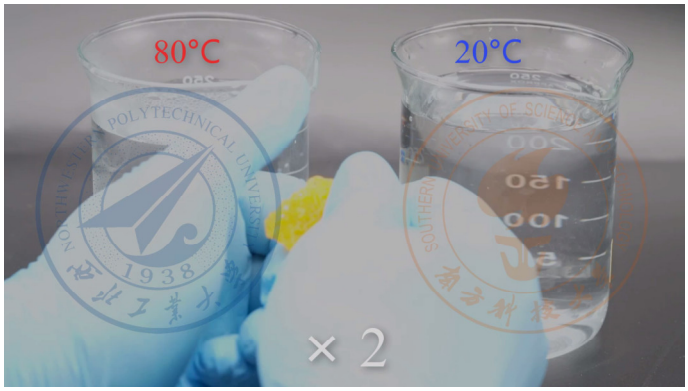

Movie S6. Shape memory process of a printed Kelvin form under complex deformations.

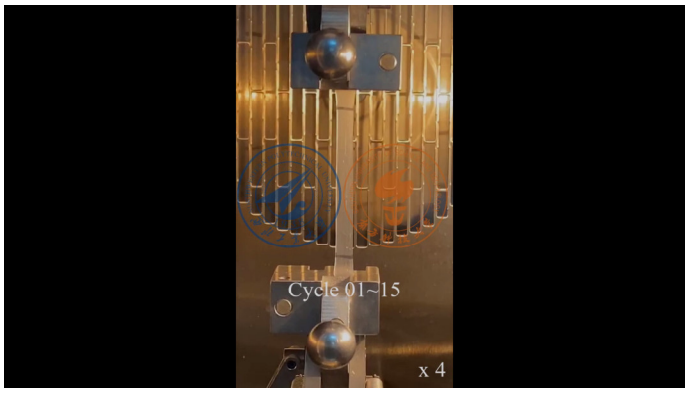

Movie S7. Fatigue test on a tBA-AUD SMP sample with 10 wt.% of AUD.

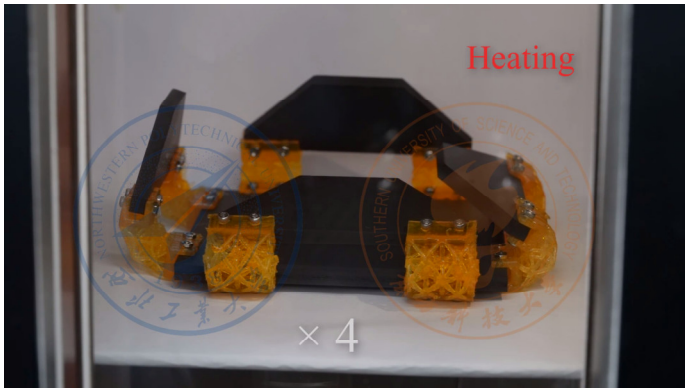

Movie S8. Recovery of a compacted smart table upon heating.

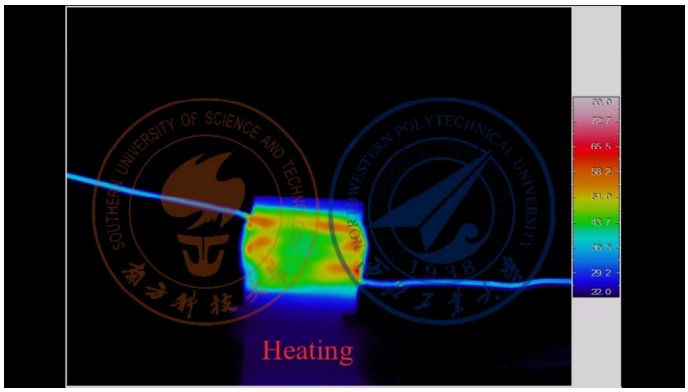

Movie S9. Recovery of a smart SMP hinge by Joule heating.

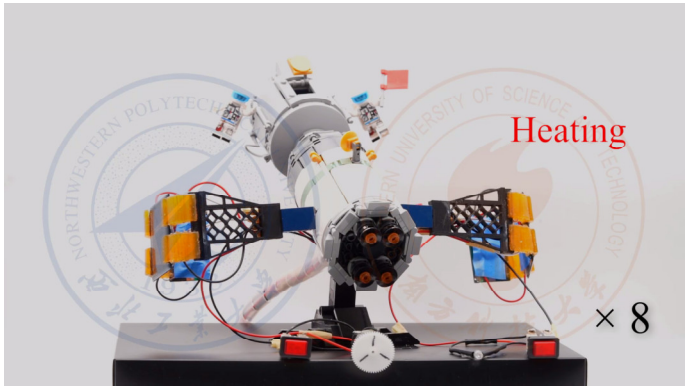

Movie S10. Depolyment of solar panels on a spacecraft.

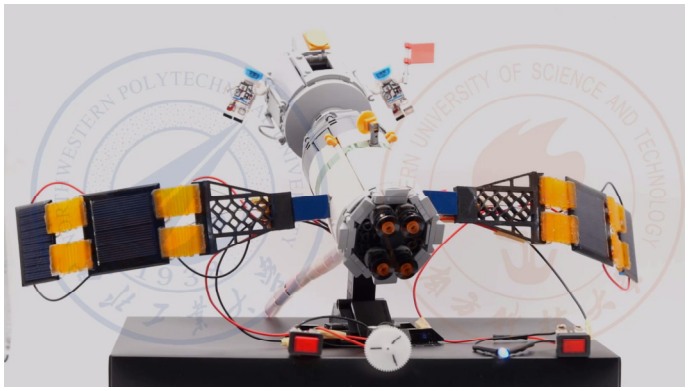

Movie S11. Demonstration of powering electronics by solar pannels.